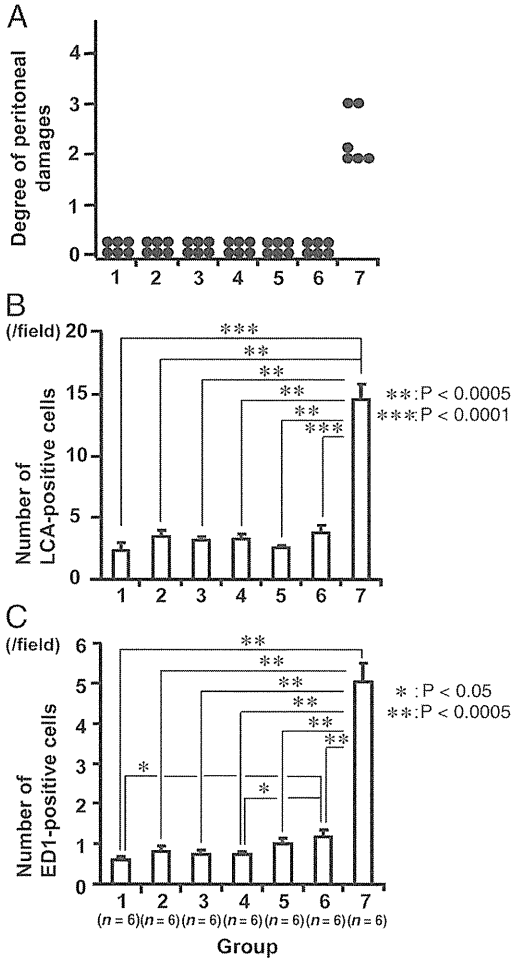

Fig. 4. Semi-quantification of peritoneal injuries and accumulation of inflammatory cells at 24 h after neutralization of CRegs. Severity of peritoneal injuries is shown as degree of severity based on pathological scoring in Groups 1 (vehicle), 2 (anti-Crry), 3 (anti-CD55), 4 (anti-CD59), 5 (anti-Crry + anti-CD55), 6 (anti-CD55 + anti-CD59) and 7 (anti-Crry + anti-CD59) (**A**). The detailed description of scoring is in the text. To evaluate accumulation of inflammatory cells, LCA-positive cells (total leukocytes) and ED-1 positive cells were counted (**B** and **C**). The data are shown as mean ± SE. *P < 0.05, **P < 0.0005 and ***P < 0.0001.

Statistical analysis

Data displayed are the mean ± SE. Statistical analysis was performed by Kruskal–Wallis test and unpaired *t*-test for cell counts. Tissue damage was analyzed by the non-parametric Mann–Whitney *U*-test. P-values < 0.05 (5%) between two groups were considered significant.

Results

Macroscopic and LM findings after suppression of CRegs

Administrated anti-CReg mAbs bound in rat peritoneum (Supplementary 2; Figure 1). Macroscopic findings in rats 24 h after administration of any single mAb or most pairs of mAbs were unremarkable with no significant macroscopic changes (Figure 2A). In contrast, in rats given a combination of mAb against Crry and CD59 (Group 7), the parietal peritoneum was edematous with white stripe-like changes, the mesentery and the visceral peritoneum were dotted with white granules and adhesion of omentum and sclerotic changes were found in the retroperitoneum of the posterior abdominal wall (Figure 2B). Additionally, rats in Group 7 had obvious peritoneal effusion at 24 h after functional suppression of Crry and CD59, while there was zero or trace peritoneal effusion after CReg functional suppression in other groups (1 to 6; Table 2).

In parietal peritoneum under LM, only Group 7 rats showed significant changes. There was accumulation of inflammatory cells, irregularity of peritoneal surface, necrotic changes in peritoneal fatty tissues and muscle destruction in sub-peritoneum in the segmental parietal peritoneum (Figure 3G). In the other groups, there were no significant pathological changes or trace cellular accumulation under the parietal peritoneum (Figures 3A–F). Peritoneal damage under LM was semi-quantitatively estimated in all groups (Figure 4A). Of note, in Group 7 rats, neither pathological changes under LM (Figures 5A–D) nor significant IgG binding (Figures 5I–L) was seen in heart, lung, liver and kidney, although parietal injury and IgG deposition were observed in this group (Figure 1G).

To observe the time course of peritoneal injury in Group 7 rats, we also examined parietal peritoneum at 6 and 72 h after neutralization of CRegs. At 6 h, there were no obvious macroscopic or microscopic changes in the parietal membrane. At 72 h, the peritoneal injuries were largely resolved with only minor residual injuries remaining (data not shown).

C deposition and tissue damage after the functional suppression of CRegs

Trace deposition of C3, but no MAC deposition, was found along the mesothelial cell layer in untreated rat peritoneum (Figures 6L and P). At 24 h, neutralization of any single CReg and any combination of two CRegs, except for the combination of Crry and CD59 (Group 7), did not induce significant deposition of C3 or MAC compared with untreated rats (Figures 6A–J, M and N). At 24 h in Group 7, abundant deposits of C3 and MAC were found in damaged tissues, including subperitoneal muscle and peritoneal surface (Figures 6K and O and Table 2).

Although no obvious macroscopic and microscopic pathological changes were found at 6 h in Group 7, abundant C3 and MAC deposits were observed on the peritoneal surface and in the sub-mesothelial layer at this time (data not shown). In other groups, only trace C3 deposition along the mesothelial layer was found at 6 h, similar to untreated rats. In Group 7, C3 and MAC deposition was reduced at 72 h, correlating with the reduced tissue damage in peritoneum in Group 7 at 72 h (data not shown).

Accumulation of inflammatory cells in peritoneum

Accumulation of inflammatory cells was compared in Groups 1 to 7 at 24 h. Figures 4B and C shows that numbers of LCA-positive and ED-1 positive cells were significantly increased in Group 7 (Crry and CD59 blocked) compared with the other groups.

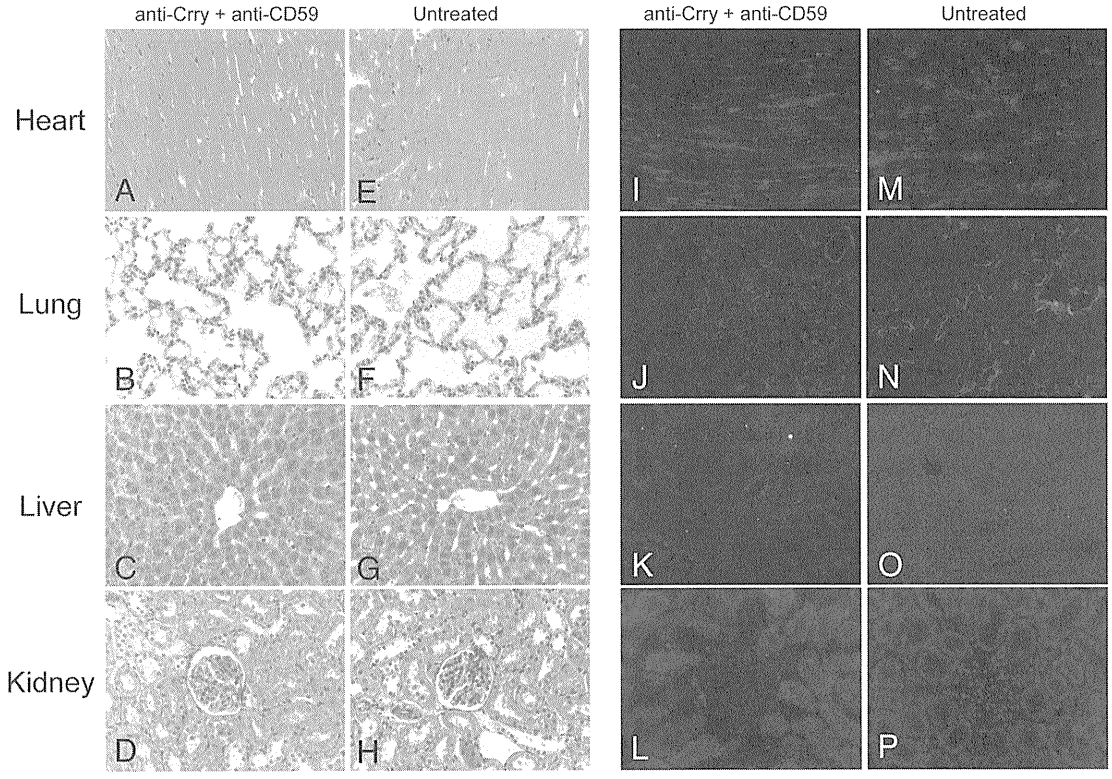

Fig. 5. Light microscopy changes and mAb deposition in heart, lung, liver and kidney after i.p. injection of anti-Crry and anti-CD59. The frames **A** to **H** show microscopic findings and **I** to **P** show immunofluorescent findings using anti-mouse IgG to detect the i.p. injected mAbs. The frames A, B, C, D, I, J, K and L show tissues 2 h after administration of anti-Crry and anti-CD59 and the frames E, F, G, H, M, N, O and P show tissues of untreated rats. No detectable pathological changes were observed in heart (A and E), lung (B and F), liver (C and G) and kidney (D and H) in experimental or control rats. No binding of anti-mouse IgG was found in heart (I and M), lung (J and N) and liver (K and O), while kidney showed trace staining in a glomerular distribution. Original magnification is ×400.

Effects of systemic C depletion by pretreatment with CVF

At 24 h after neutralization of Crry and CD59, no macroscopic changes were observed in CVF-pretreated rats (Group 8) while marked macroscopic changes and abundant peritoneal effusion were found in the control group (Group 9) (Figure 7). Under LM, similar pathological changes to those described in Group 7 were observed in control Group 9 (Figure 7D), while no significant peritoneal injuries were found following systemic C depletion (Figure 7A). No C3 or MAC was deposited in peritoneum in Group 8 (Figures 7B and C), although abundant C3 and MAC deposition was observed along injured peritoneum in Group 9 controls (Figure 7E and F). Accumulation of inflammatory cells in peritoneum was also suppressed in Group 8 compared with Group 9 (Figures 7H and I).

C3 deposition after suppression of CRegs on rat mesothelial cells

Treatment of cells with single mAbs or most pairs of mAbs together with RS caused no increase in C3 deposition compared with RS only (Figure 8C). In contrast, RS combined with mAb against Crry and CD59 induced remarkable C3 deposition on mesothelial cells (Figure 8B and E). Heat-inactivated RS, with or without mAbs, did not cause C3 deposition on cells (Figure 8D).

Effect of different pH and osmotic conditions on C3 deposition in rat mesothelial cells following neutralization of Crry and CD59

Peritoneal injuries and accumulation of infiltrated cells in rat peritoneum at 24 h post-neutralization of Crry and CD59 were assessed at different levels of pH and glucose concentration. Macroscopic changes in the peritoneum of rats treated with neutralizing mAbs in PD2 4.25% (pH ~5) were the most widespread and severe among the four PD solutions tested, while mAbs in PBS caused the least injury (Figure 9A–C). To confirm the influence of acidic pH or glucose as an osmotic stress, we assessed C3 deposition on rat mesothelial cells treated with RS in pH 5.0, 5.4, 6.4 or 7.4 M199 medium after suppression of Crry and CD59 or in 0, 1.5, 2.5 or 4.25% glucose contained in M199 medium. C3 deposition was lowest at pH 7.4 and increased at lower pH (Figure 9D). C3 deposition on cells was significantly greater in 2.5% and 4.25% glucose compared to 0% glucose concentration in the medium (Figure 9E).

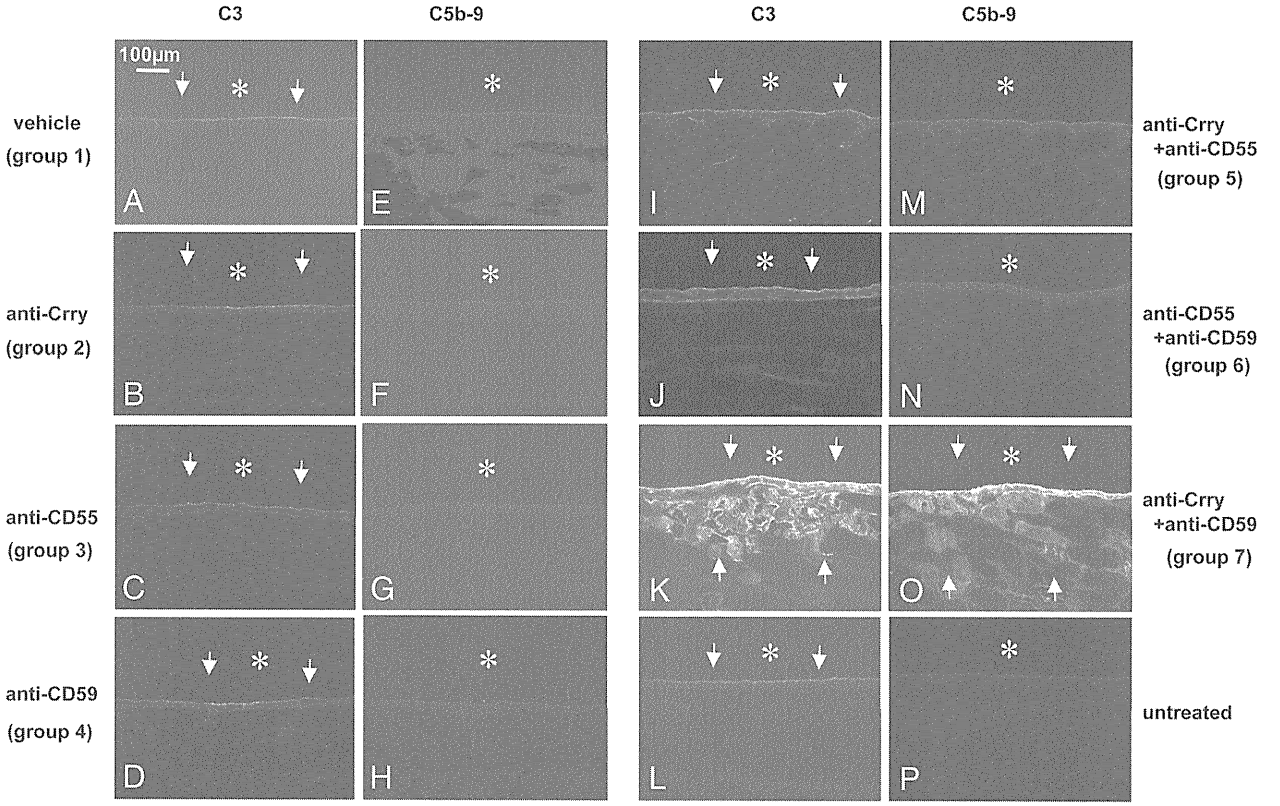

Fig. 6. C3 and C5b-9 deposition in parietal peritoneum at 24 h after neutralization of CRegs. C3 deposition is shown in frames **A** to **D** and **I** to **L**, while C5b-9 deposition is shown in frames **E** to **H** and **M** to **P**. The pairs of frames show A/E, Group 1 (vehicle); B/F, Group 2 (anti-Crry); C/G, Group 3 (anti-CD55); D/H, Group 4 (anti-CD59); I/M, Group 5 (anti-Crry + anti-CD55); J/N, Group 6 (anti-CD55 + anti-CD59); K/O, Group 7 (anti-Crry + anti-CD59); and L/P, untreated control. The peritoneal surface was labelled as '*'. Arrowheads show the positive binding sites. Original magnification is × 200. The bar in the left-upper corner in frame A is shown as scale of 100 μm.

Discussion

In our recent report [18], we showed that the CRegs Crry, CD55 and CD59 were expressed in rat peritoneum, but CD46 was not expressed. Therefore, we here investigated functional roles of CRegs, Crry, CD55 and CD59, by blocking with specific mAb in the presence of PDF. Neutralization of individual CReg, Crry, CD55 or CD59, in rat peritoneum did not cause significant tissue damage in the peritoneum. These findings were different from those reported in other tissues [1–3,5,18,24]. When we blocked a specific combination of two CRegs, Crry and CD59, in the peritoneum, acute and transient peritonitis was induced. Although anti-CRegs might in themselves cause some C activation, this is unlikely to be significant because neither single nor any other combination of two anti-CRegs caused any significant inflammation in the peritoneum. Local production of complement has been reported in peritoneum [11–14], and CRegs likely regulate local C activation. The inflammation induced by blockade of Crry and CD59 was prevented by systemic C depletion with CVF, confirming its C dependence. We could not distinguish local C production from systemic C delivery, both local and systemic C likely contribute to the peritoneal injuries. Systemic effects of i.p. injected mAbs anti-Crry and anti-CD59 were minimal as demonstrated by lack of binding of mAbs and no microscopic injuries in other tissues.

These findings showed that C regulation by CRegs contributes to the maintenance of homeostasis in the normal peritoneum, as shown in other tissues. It was interesting that neutralization of no single CReg induced inflammation in rat peritoneum, only simultaneous neutralization of Crry and CD59 induced inflammation, suggesting that homeostatic C regulation was achieved through a combination of Crry and CD59 in rat peritoneum. Although CD55 is also a C3 level C regulator, Crry is the dominant regulator of this step; consequently, blocking CD55 alone or a combination of CD55 and CD59 did not induce peritoneal injuries while Crry remained active. The peritoneal cavity is usually a sterile environment. However, there are opportunities, particularly in the context of PD, for the environment to be contaminated by microorganisms. It might therefore be essential for tick-over low-level complement activation to occur in the normal peritoneum to maintain homeostasis and provide the primary defense against microorganism invasion. In support of this concept is the trace C3b distribution along the normal peritoneal surface. Collaboration of CRegs in the peritoneum would then be important to regulate this physiological C activation. At the C3 level in rat peritoneum, Crry is the key CReg because neutralization of Crry was essential to induce peritoneal inflammation, but additional neutralization of CD59 was required to develop peritonitis. CD55, another C3 level

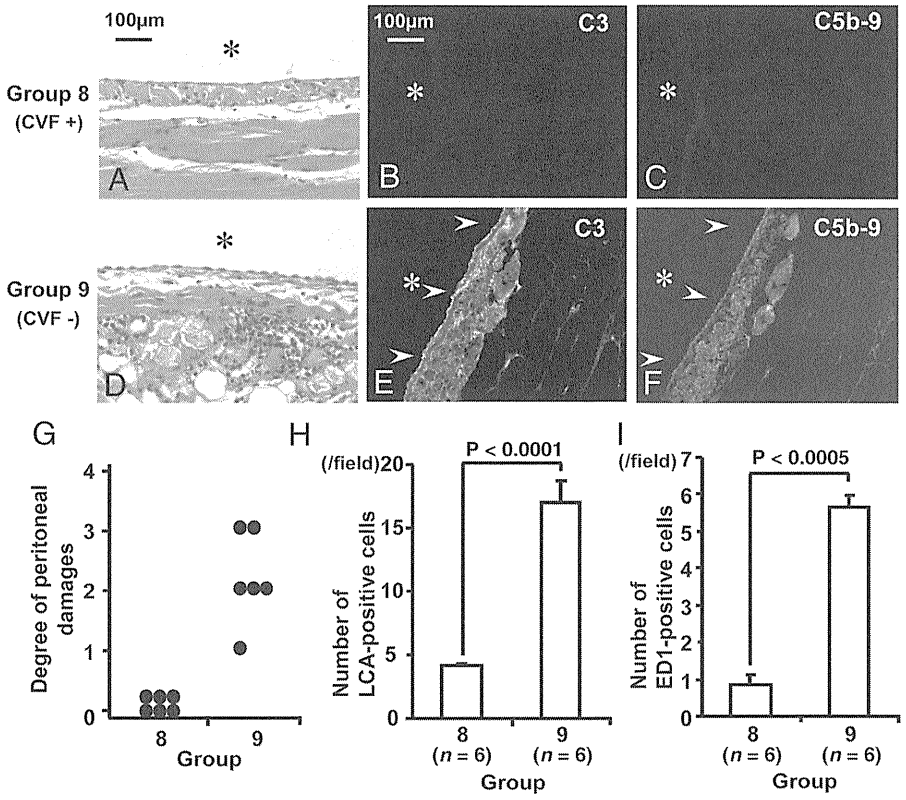

Fig. 7. Effects of functional blockade of Crry and CD59 following depletion of systemic complement. Frames **A** and **D** are LM photos and frames **B**, **C**, **E** and **F** are IF photos. Frames A, B and C are from CVF-treated animals (Group 8) and frames D, E and F are from animals not pretreated with CVF (Group 9). The peritoneal surface was labelled as '*'. Arrowheads show the positive binding sites. Original magnification from A to F is ×200, and the scale bar of 100 μm is shown in frames A and B. Graph **G** shows a comparison of the degree of peritoneal damage between groups 8 and 9. Graphs **H** and **I** show comparisons of inflammatory cell accumulation in peritoneum.

CReg expressed in peritoneum, was not critical to peritoneal integrity, as its neutralization, alone or with either Crry or CD59, did not result in peritoneal injury.

Our *in vitro* results using rat mesothelial cells support the *in vivo* results, showing that regulation both in the activation pathways and the terminal pathway is required for homeostasis, a finding that may have relevance for the therapeutic use of C inhibitors. The findings imply that spontaneous C activation in peritoneum is essential in defense against infection and that low C levels in peritoneal fluid, for example in liver cirrhosis [25], might predispose to disease, particularly spontaneous bacterial peritonitis [26,27].

We investigated the effects of Crry and CD59 neutralization under four different conditions: PBS (isotonic and neutral pH), NPD4 1.5% (moderate high osmotic and close to neutral pH), PD4 1.5% and PD4 4.25% (high osmotic and low pH). Peritonitis induced by neutralization of Crry and CD59 in PBS was clearly milder than that induced by the same antibodies in either NPD4 1.5%, PD4 1.5% or PD4 4.25%; the latter caused the most severe peritoneal inflammation. In support of these findings, acidic PD solution caused more C3 deposition on cultured peritoneal mesothelial cells exposed to anti-Crry, anti-CD59 and RS than neutral solution, supporting the proposition that acidic pH induced higher C activation, revealed by blocking Crry and CD59.

New generation formulations of PDF are improved in terms of pH (near neutral) and/or glucose degradation products (GDPs) because low pH and high GDP levels in PDF were found to directly cause mesothelial injuries [8,28]. However, many PDFs still in clinical use are low in pH and often, because of ultrafiltration failure, hypertonic PDFs must be used in some patients. PDFs with neutral pH and low GDPs improve local peritoneal homeostasis [28]. This is in part because both low pH [8] and GDPs can activate the C system, the latter because glycated IgG enhances C activation [29]. Furthermore, high glucose PDF can cause hyperglycemia, which in turn can cause glycation inactivation of CD59 and impaired C regulation [30], or loss of CD55 and CD59 from cell membranes *in vitro* [31]. High glucose content in PDF likely causes local inactivation of CD59, further contributing to injury. From those reports, it is clear that PDF can enhance C-dependent acute peritonitis and that biocompatible dialysate is likely beneficial, as shown *in vitro* and *in vivo* in animal and human studies [32–34].

Recently, we showed that the C activation enhanced inflammation in fungal peritonitis in a rodent PD model, leading to severe and chronically progressive peritoneal inflammation [18]. The present study confirms that peritoneal C regulation is important not only to suppress peritoneal inflammation during PD therapy but also to maintain homeostasis in the peritoneal cavity.

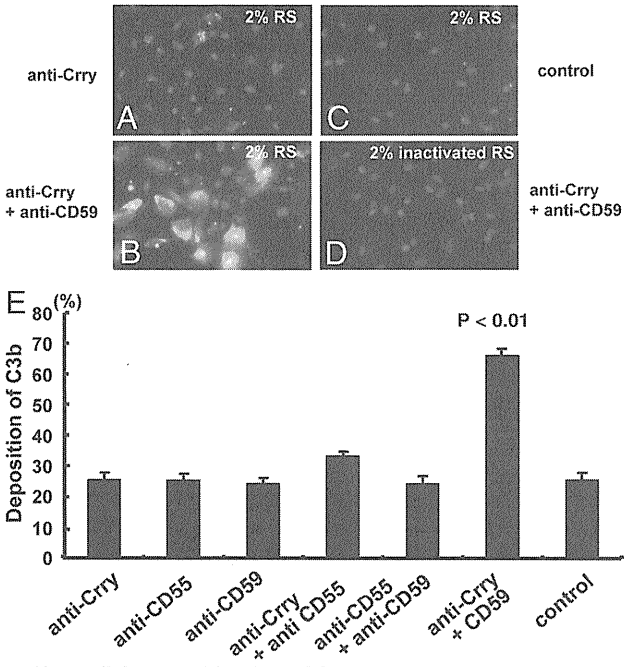

Fig. 8. C3 deposition on rat mesothelial cells with neutralization of membrane complement regulators (CRegs). Frames **A**, **B** and **C** show C3 deposition on rat mesothelial cells after incubation with 2% rat serum (RS), while frame **D** shows the cells after incubation with 2% heat-inactivated rat serum (RS). C3 deposition following incubation with any single mAb or most pairs of mAbs against CRegs, except for a combination of anti-Crry and anti-CD59, was small and similar to that seen with 2% RS without mAb (as an example, compare anti-Crry treated in A and controls in C). Frame B shows abundant C3b deposition on mesothelial cells treated with anti-Crry and anti-CD59 and incubated with RS. When mesothelial cells treated with anti-Crry and anti-CD59 were incubated with heat-inactivated RS, no significant C3 deposition was seen (D). Figure 8E quantifies the degree of C3 deposition on mesothelial cells treated with the different mAb combinations and incubated with RS.

Supplementary data

Supplementary data is available online at http://ndt.oxfordjournals.org.

Acknowledgements. The authors thank Suzuki, Asano and Fujitani for technical help. This work was supported in part by grant-in-aids for Scientific Research from the Ministry Education, Science, and Culture, Japan (#19590946 and #21591054) and by the 2008 research grant from the Aichi Kidney Foundation. Morgan is supported by The Wellcome Trust (Programme no. 068590).

Conflict of interest statement. None declared.

References

1. Mizuno M, Morgan BP. The possibilities and pitfalls for anti-complement therapies in inflammatory diseases. *Curr Drug Targets Inflamm Allergy* 2004; 3: 87–96
2. Nishikawa K, Matsuo S, Okada N *et al.* Local inflammation caused by a monoclonal antibody that blocks the function of the rat membrane inhibitor of C3 convertase. *J Immunol* 1996; 156: 1182–1188
3. Nomura A, Nishikawa K, Yuzawa Y *et al.* Tubulointerstitial injury induced in rats by a monoclonal antibody that inhibits function of a membrane inhibitor of complement. *J Clin Invest* 1995; 96: 2348–2356
4. Bardenstein DS, Cheyer CJ, Lee C *et al.* Blockage of complement regulators in the conjunctiva and within the eye leads to massive inflammation and iritis. *Immunology* 2001; 104: 423–430
5. Mizuno M, Nishikawa K, Goodfellow RM *et al.* The effects of functional suppression of a membrane-bound complement regulatory protein, CD59, in the synovial tissue in rats. *Arthritis Rheum* 1997; 40: 527–533
6. Watanabe M, Morita Y, Mizuno M *et al.* CD59 protects rat kidney from complement mediated injury in collaboration with crry. *Kidney Int* 2000; 58: 1569–1579
7. Mizuno M, Nishikawa K, Spiller OB *et al.* Membrane complement regulators protect against the development of type II collagen-induced arthritis in rats. *Arthritis Rheum* 2001; 44: 2425–2434
8. Lardner A. The effects of extracellular pH on immune function. *J Leukoc Biol* 2001; 69: 522–530
9. Topley N, Kaur D, Petersen MM *et al.* In vitro effects of bicarbonate and bicarbonate-lactate buffered peritoneal dialysis solutions on mesothelial and neutrophil function. *J Am Soc Nephrol* 1996; 7: 218–224
10. Liberek T, Topley N, Jorres A *et al.* Peritoneal dialysis fluid inhibition of phagocyte function: effects of osmolality and glucose concentration. *J Am Soc Nephrol* 1993; 3: 1508–1515
11. Young GA, Kendall S, Brownjohn AM. Complement activation during CAPD. *Nephrol Dial Transplant* 1993; 8: 1372–1375
12. Tang S, Leung JC, Chan LY *et al.* Regulation of complement C3 and C4 synthesis in human peritoneal mesothelial cells by peritoneal dialysis fluid. *Clin Exp Immunol* 2004; 136: 85–94
13. Reddingius RE, Schroder CH, Daha MR *et al.* Complement in serum and dialysate in children on continuous ambulatory peritoneal dialysis. *Perit Dial Int* 1995; 15: 49–53
14. Kabut J, Kondera-Anasz Z, Sikora J *et al.* Levels of complement components iC3b, C3c, C4, and SC5b-9 in peritoneal fluid and serum of infertile women with endometriosis. *Fertil Steril* 2007; 88: 1298–1303
15. Lam MF, Leung JC, Tang CC *et al.* Mannose binding lectin level and polymorphism in patients on long-term peritoneal dialysis. *Nephrol Dial Transplant* 2006; 21: 1729–1730
16. Barbano G, Cappa F, Prigione I *et al.* Peritoneal mesothelial cells produce complement factors and express CD59 that inhibits C5b-9-mediated cell lysis. *Adv Perit Dial* 1999; 15: 253–257
17. Mizuno M, Harris CL, Johnson PM *et al.* Rat membrane cofactor protein (MCP; CD46) is expressed only in the acrosome of developing and mature spermatozoa and mediates binding to immobilized activated C3. *Biol Reprod* 2004; 71: 1374–1383
18. Mizuno M, Ito Y, Hepburn N *et al.* Zymosan, but not lipopolysaccharide, triggers severe and progressive peritoneal injury accompanied by complement activation in a rat peritonitis model. *J Immunol* 2009; 183: 1403–1412
19. Hughes TR, Piddlesden SJ, Williams JD *et al.* Isolation and characterization of a membrane protein from rat erythrocytes which inhibits lysis by the membrane attack complex of rat complement. *Biochem J* 1992; 284: 169–176
20. Spiller OB, Hanna SM, Morgan BP. Tissue distribution of the rat analogue of decay-accelerating factor. *Immunology* 1999; 97: 374–384
21. Mizuno M, Harris CL, Suzuki N *et al.* Expression of CD46 in developing rat spermatozoa: ultrastructural localization and utility as a marker of the various stages of the seminiferous tubuli. *Biol Reprod* 2005; 72: 908–915
22. Ota T, Kuwahara M, Fan S *et al.* Expression of aquaporin-1 in the peritoneal tissues: localization and regulation by hyperosmolality. *Perit Dial Int* 2002; 22: 307–315
23. Kaifu K, Kiyomoto H, Hitomi H *et al.* Insulin attenuates apoptosis induced by high glucose via the PI3-kinase/Akt pathway in rat peritoneal mesothelial cells. *Nephrol Dial Transplant* 2009; 24: 809–815
24. Mizuno M, Nishikawa K, Okada N *et al.* Inhibition of a membrane complement regulatory protein by a monoclonal antibody induces acute lethal shock in rats primed with lipopolysaccharide. *J Immunol* 1999; 162: 5477–5482
25. Ljubicic N, Bilic A, Kopjar B. Diuretics vs. paracentesis followed by diuretics in cirrhosis: effect on ascites opsonic activity and im-

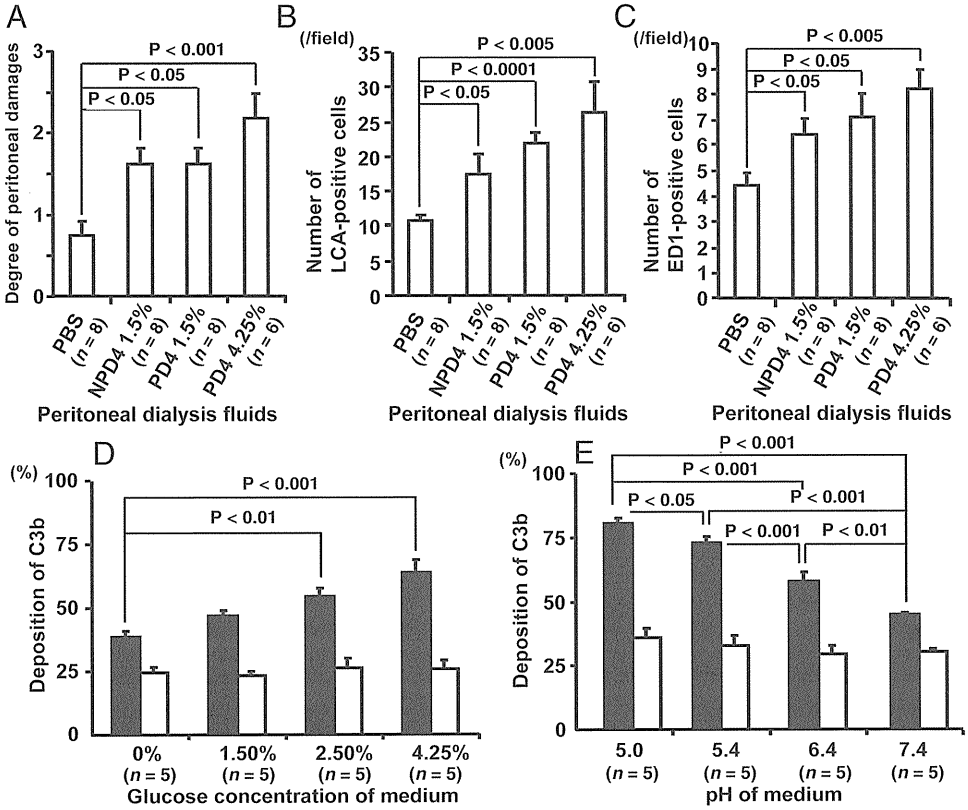

Fig. 9. Peritoneal injury, accumulation of inflammatory cells and mesothelial cell injury after neutralization of Crry and CD59 in PBS or peritoneal dialysate fluids. Severity of peritoneal injury, based on pathological scoring as described in text, in rats treated with anti-Crry and anti-CD59 delivered in PBS, NPD4 1.5%, PD4 1.5% or NP4 4.25% (**A**). To evaluate accumulation of inflammatory cells, LCA-positive and ED-1 positive cells in peritoneal tissue were counted (**B** and **C**). Plate **D** shows the degree of C3 deposition on mesothelial cells after mAb neutralization of Crry and CD59 in pH 5.0, 5.4, 6.4 or 7.4 M199 medium solution (closed hatch), while open hatch shows C3 deposition on the cells exposed to the medium alone. Plate **E** shows the degree of C3 deposition on mesothelial cells after mAb neutralization of Crry and CD59 in 0, 1.50, 2.50 or 4.25% of glucose in M199 medium solution (closed hatch), while open hatch shows C3 deposition on the cells exposed to the medium alone. The data are shown as mean ± SE.

munoglobulin and complement concentrations. *Hepatology* 1994; 19: 346–353
26. Such J, Guarner C, Soriano G *et al.* Selective intestinal decontamination increases serum and ascitic fluid C3 levels in cirrhosis. *Hepatology* 1990; 12: 1175–1178
27. Chen SM, Lo GH, Lai KH *et al.* Serum and ascitic concentration of C3, C4 and protein in cirrhotic patients with spontaneous bacterial peritonitis. *Zhonghua Yi Xue Za Zhi* 1994; 54: 87–92
28. Williams JD, Topley N, Craig KJ *et al.* The Euro-Balance Trial: the effect of a new biocompatible peritoneal dialysis fluid (balance) on the peritoneal membrane. *Kidney Int* 2004; 66: 408–418
29. Davin JC, Bouts AH, Krediet RT *et al.* IgG glycation and function during continuous ambulatory peritoneal dialysis. *Nephrol Dial Transplant* 1997; 12: 310–314
30. Davies CS, Harris CL, Morgan BP. Glycation of CD59 impairs complement regulation on erythrocytes from diabetic subjects. *Immunology* 2005; 114: 280–286
31. Accardo-Palumbo A, Triolo G, Colonna-Romano G *et al.* Glucose-induced loss of glycosyl-phosphatidylinositol-anchored membrane regulators of complement activation (CD59, CD55) by in vitro cultured human umbilical vein endothelial cells. *Diabetologia* 2000; 43: 1039–1047
32. Jörres A, Bender TO, Finn A *et al.* Biocompatibility and buffers: effect of bicarbonate-buffered peritoneal dialysis fluids on peritoneal cell function. *Kidney Int* 1998; 54: 2184–2193
33. Fabbrini P, Zareie M, Ter Wee PM *et al.* Peritoneal exposure model in the rat as a tool to unravel bio(in)compatibility of PDF. *Nephrol Dial Transplant* 2006; 21: ii8–ii11
34. Lee HY, Park HC, Seo BJ *et al.* Superior patient survival for continuous ambulatory peritoneal dialysis patients treated with a peritoneal dialysis fluid with neutral pH and low glucose degradation product concentration (Balance). *Perit Dial Int* 2005; 25: 248–255

Received for publication: 8.4.10; Accepted in revised form: 14.10.10

The American Journal of Pathology, Vol. 178, No. 2, February 2011

DOI: 10.1016/j.ajpath.2010.10.009

Cardiovascular, Pulmonary, and Renal Pathology

Basigin/CD147 Promotes Renal Fibrosis after Unilateral Ureteral Obstruction

Noritoshi Kato,*† Tomoki Kosugi,*† Waichi Sato,† Takuji Ishimoto,† Hiroshi Kojima,† Yuka Sato,† Kazuma Sakamoto,* Shoichi Maruyama,† Yukio Yuzawa,† Seiichi Matsuo,† and Kenji Kadomatsu*

From the Departments of Biochemistry and Nephrology of Internal Medicine,† Nagoya University Graduate School of Medicine, Nagoya, Japan*

Regardless of their primary causes, progressive renal fibrosis and tubular atrophy are the main predictors of progression to end-stage renal disease. Basigin/CD147 is a multifunctional molecule–it induces matrix metalloproteinases and hyaluronan, for example–and has been implicated in organ fibrosis. However, the relationship between basigin and organ fibrosis has been poorly studied. We investigated basigin's role in renal fibrosis using a unilateral ureteral obstruction model. Basigin-deficient mice (*Bsg*$^{-/-}$) demonstrated significantly less fibrosis after surgery than *Bsg*$^{+/+}$ mice. Fewer macrophages had infiltrated in *Bsg*$^{-/-}$ kidneys. Consistent with these *in vivo* data, primary cultured tubular epithelial cells from *Bsg*$^{-/-}$ mice produced less matrix metalloproteinase and exhibited less motility on stimulation with transforming growth factor β. Furthermore, *Bsg*$^{-/-}$ embryonic fibro blasts produced less hyaluronan and α-smooth muscle actin after transforming growth factor β stimulation. Together, these results demonstrate for the first time that basigin is a key regulator of renal fibrosis. Basigin could be a candidate target molecule for the prevention of organ fibrosis. *(Am J Pathol 2011, 178:572–579; DOI: 10.1016/j.ajpath.2010.10.009)*

Regardless of the primary disease process, renal interstitial fibrosis is the key determinant of chronically diseased kidney and the main prognostic predictor of renal function.[1] Excessive accumulation of extracellular matrix (ECM) leads to dysfunction of the organ and state of fibrosis.[2] ECM turnover is regulated by the activity of matrix metalloproteinases (MMPs). Although transforming growth factor β (TGF-β) stimulates α-SMA expression as well as ECM production by fibroblasts, it also regulates the expression of MMPs.[3,4] Conversely, some MMPs, such as MMP-2, MMP-9, and MT1-MMP, activate latent TGF-β.[5,6] Therefore, ECM synthesis and degradation are intricately regulated by TGF-β, MMPs, and others. In this context, it should also be noted that hyaluronan plays a crucial role in the TGF-β–driven differentiation of fibroblasts into myofibroblasts.[7–10] Endogenous hyaluronan is necessary for fibroblast differentiation and maintenance of the myofibroblast phenotype through autocrine TGF-β action.[11]

Basigin (Bsg)/CD147 (*Bsg* is the name of the mouse gene) is a glycosylated transmembrane protein that belongs to the immunoglobulin superfamily. It is expressed by many types of cells, including hematopoietic, epithelial, endothelial, and tumor cells.[12,13] It is well documented that Bsg induces MMPs, so it is also known as an extracellular matrix metalloproteinase inducer (EMMPRIN).[14] It is highly up-regulated in many malignant cancer cells and is thought to contribute to cell survival, invasion, metastasis, and multidrug resistance.[15] Studies targeting Bsg to prevent tumor growth using RNAi techniques have achieved successful outcomes.[16–19] Along with MMPs, Bsg is also involved in the production of vascular endothelial growth factor and hyaluronan.[20–24] Bsg interacts with a wide range of binding partners.[25] For example, it binds to caveolin, cyclophilin, monocarboxylate transporter, and Bsg itself.[26–29] Through the interaction with monocarboxylate transporter, Bsg plays a role in lactate metabolism. Furthermore, Bsg promotes the differentiation of fibroblasts into myofibroblasts by inducing α-SMA expression in corneal fibroblasts.[30]

We previously generated Bsg-deficient mice (*Bsg*$^{-/-}$) and reported several abnormalities, including male and female sterility, progressive retinal degeneration, increased cell proliferation on mixed lymphocyte culture, decreased

Supported by Grants-in-Aid from the Ministry of Education, Culture, Sports, Science, and Technology of Japan (the global COE program to Nagoya University).

Accepted for publication October 1, 2010.

N.K. and T.K. contributed equally to this work.

Address reprint requests to Kenji Kadomatsu, M.D., Ph.D., Department of Biochemistry, Nagoya University Graduate School of Medicine, 65 Tsurumai-cho, Showa-ku, Nagoya 466-8550, Japan. E-mail: kkadoma@med.nagoya-u.ac.jp.

memory function, and abnormal sensory function.[31–33] Most recently, we also found that Bsg is an E-selectin ligand and is involved in renal ischemia/reperfusion injury.[34]

In this study, we focused on Bsg functions in renal fibrosis induced by unilateral ureteral obstruction (UUO). Bsg orchestrates renal fibrosis formation through MMPs, hyaluronan production, and macrophage infiltration. To the best of our knowledge, this is the first report on the critical role of Bsg in renal fibrosis.

Materials and Methods

Animals and Experimental Design

Mice deficient in *Bsg* were generated as described previously.[35] Because $Bsg^{-/-}$ mice were hardly born through ordinary mating, we established the following protocol. $Bsg^{+/-}$ mice with 129/SV background were backcrossed with C57BL/6J mice to produce F1 hybrid offspring (reverse F1 hybrid). By intercrossing these mice, mixed reverse F2 mice were generated, and were used in this study. All experiments were performed with $Bsg^{+/+}$ and $Bsg^{-/-}$ littermates. We used 96 mice (48 mice in each genotype, respectively), which were 8- to 12-week-old males weighing 20 to 25 g. These mice were divided into seven groups at each time point (n = 8/each group on day 0, 7, and 14; n = 6/each group on day 1, 2, 3, and 5, respectively). The mice were housed under controlled environmental conditions and maintained with standard food and water.

In $Bsg^{+/+}$ and $Bsg^{-/-}$ mice sedated by general anesthesia, an incision was made in the right side of the back, and complete ureteral obstruction was performed by double-ligating the right ureter using 4-0 silk. Sham-operated mice had their ureters exposed but not ligated. Mice were sacrificed at different time points as indicated after surgery. Kidneys were removed for examination. Blood and urine samples were collected on the day of sacrifice. Kidney tissues were processed for histology and protein extraction. All of the animal experiments were performed in accordance with the animal experimentation guidelines of Nagoya University School of Medicine.

Histology

The removed kidneys were fixed in 4% paraformaldehyde, embedded in paraffin, and then cut into 4-μm sections. The sections were stained with polyclonal goat anti-human type III collagen (Southern Biotech, Birmingham, AL) and polyclonal goat anti-mouse Bsg (R&D Systems, Minneapolis, MN) followed by detection with biotin-conjugated rabbit anti-goat IgG (Nichirei, Tokyo, Japan). Immunostaining was performed by the streptavidin (Chemicon International, Temecula, CA) -biotin immunoperoxidase method. The staining was visualized with 3,3′-diaminobenzidine (Dako, Carpinteria, CA), a brown color being produced. Negative controls involved replacement of the primary antibodies with species-matched antibodies.

The sections were stained with periodic acid-Schiff reagent (PAS). Tubular dilation was assessed by counting the number of dilated tubules in the cortex of each section.[36] They were also stained with a terminal deoxynucleotidyl transferase-mediated dUTP nick-end labeling (TUNEL) assay kit according to the manufacturer's instructions (Roche Applied Science, Indianapolis, IN). The number of apoptotic cells was examined in the cortex of each section.

Parts of the kidney tissues were snap-frozen in liquid nitrogen. Sections (2-μm thick) were cut with a cryostat and then fixed in acetone. The cryosections were stained with rat anti-mouse monocyte-macrophage marker F4/80 (Serotec, Oxford, UK) followed by detection with fluorescein isothiocyanate rabbit anti-rat IgG (Zymed Laboratories, San Francisco, CA). Macrophages positive for F4/80 were counted by examining 10 fields of the cortex under a microscope at ×200 magnification in a blind manner.

Real-Time PCR

Mouse kidney tissues were snap-frozen in liquid nitrogen for total mRNA isolation. To perform mRNA extraction and cDNA synthesis, we used the RNeasy Mini Kit and QuantiTect Reverse Transcriptional Kit (Qiagen, Hilden, Germany) according to the manufacturer's instructions. Real-time PCR analysis was performed with an Applied Biosystems Prism 7500HT sequence detection system using TaqMan gene expression assays according to the manufacturer's specifications (Applied Biosystems, Foster City, CA). TaqMan probes and primers for type III collagen (Col3a1; Mm00802331_m1), TGF-β_1 (*Tgfb1*; Mm00441724_m1), hyaluronan synthase 2 (*Has2*; Mm00515089_m1), α-SMA (*Acta2*; Mm01546133_m1), β-actin (*Actb*; Mm00607939_s1), and glyceraldehyde-3-phosphate dehydrogenase (*Gapdh*; Mm99999915_g1) were used. Amplification data were analyzed with Applied Biosystems Sequence Detection software version 1.3.1.

Western Blot Analysis

Mouse kidney tissues were snap-frozen in liquid nitrogen for protein isolation and then lysed in radio-immunoprecipitation assay buffer (50 mmol/L Tris-HCl, 150 mmol/L NaCl, 1% Nonidet P, 1% deoxycolic acid, and 0.05% SDS). Western blot analysis was performed as described previously.[37]

Briefly, we separated the samples by 10% SDS-PAGE and then transferred them to a nitrocellulose membrane (Whatman, Florham Park, NJ). We blocked the membranes with 5% (w/v) dry fat-free milk in PBS with 0.1% Tween for 60 minutes at room temperature. The blots were subsequently incubated with goat anti-mouse Bsg antibody (R&D Systems), monoclonal anti-β actin antibody (Sigma Aldrich, St. Louis, MO), or rat anti-mouse E-selectin antibody (R&D Systems), followed by incubation with peroxidase-conjugated anti-goat IgG, rat IgG, and mouse IgG (Jackson Immunoresearch Laboratories, West Grove, PA). Proteins were visualized with an enhanced chemiluminescence detection system (Amersham Pharmacia, Amersham Biosciences, Piscataway, NJ). The density of each band was measured using the public domain National Institutes of Health image program.

Gelatin Zymography

Kidney tissue homogenates and cultured media of TECs were subjected to gelatin zymography of the MMP proteolytic activity. Gelatin zymography was performed using commercial kit (Invitrogen, Carlsbad, CA) according to the manufacturer's instructions. Briefly, the homogenates were loaded into 7.5% SDS-polyacrylamide gel containing 1 mg/ml gelatin. After electrophoresis, the gel was incubated in 2.5% Triton X-100 at room temperature for 30 minutes with gentle shaking and then at 37°C for 24 hours in a developing buffer containing $CaCl_2$ Tris-HCl. The gel was stained with Coomassie blue. Proteinase activity was detected as unstained bands on a blue background, representing areas of gelatin digestion. The density of each band was measured using the public-domain National Institutes of Health image program.

Cell Culture

Tubular epithelial cells (TECs) were isolated from the kidneys of adult $Bsg^{+/+}$ or $Bsg^{-/-}$ mice, as described previously.[38] Briefly, the renal cortex divided from the medulla was resolved with collagenase (Wako Chemicals, Miyazaki, Japan) and the lysate was then filtered through 38-μm strainer, using a mesh sieving method. The fluid was centrifuged to pellet the various renal cells, which were plated with cultured media for 1 hour of incubation. To avoid the contamination of mesangial cells and various cells, adherent cells were removed, and a supernatant solution including numerous TECs was incubated to another plate for 72 hours in K1 medium [224.25 ml Ham's F12; 226.25 ml Dulbecco's modified Eagle's medium (DMEM); and 12.5 ml HEPES] containing 10% fetal bovine serum (GIBCO BRL, Gaithersburg, MD) and hormones [epidermal growth factor (50 pg/ml); insulin-transferrin-sodium selenite media supplement (0.12 IU/ml), prostaglandin E_1 (1.25 ng/ml), hydrocortisone (18 ng/ml); T3 (34 pg/ml)]. The fourth and fifth passages were used for experiments. These cells isolated from the kidneys were determined to be of proximal tubular origin by means of immunofluorescence histochemistry; cells were stained positively for cytokeratin (ENZO Diagnostics, Farmingdale, NY); brush border vesicle (BBV; gift from Dr. G. Andres)[39]; desmin (Progen, Heidelberg, Germany), and Phalloidin (Invitrogen). These staining patterns were the same as those previously reported.[40]

Subconfluent tubular epithelial cells were incubated in serum-free medium for 24 hours to arrest and synchronize cell growth. After that, the medium was changed to fresh serum-free DMEM containing 5 ng/ml recombinant TGF-β (R&D Systems) for 0, 1, 3, 6, 12, and 24 hours in the time-course study. *The culture* medium was subjected to gelatin zymography.

Mouse embryonic fibroblast (MEF) was established from the embryos of $Bsg^{+/+}$ and $Bsg^{-/-}$ mice and then cultured in DMEM containing 10% fetal bovine serum.[41] After the cells were starved for 24 hours, the medium was changed to fresh serum-free DMEM containing 5 ng/ml recombinant TGF-β (R&D Systems). Cells were then used for the collection of mRNA, and culture medium was used for hyaluronan ELISA.

Cell Invasion Assay

To compare cell migration capacity between $Bsg^{+/+}$ TECs and $Bsg^{-/-}$, we used the Cultrex Cell Invasion/Migration Assay according to the manufacturer's instructions (Trevigen, Gaithersburg, MD) to mimic *in vivo* the tubular basement membrane microenvironment and the renal interstitium and to screen compounds that influence cellular digestion and migration across ECM. This assay used a simplified Boyden chamber design with an 8-micron polyethylene terephthalate membrane coated with basement membrane extract. The bottom wells of a 96-well Boyden chamber were filled with DMEM containing 5 ng/ml TGF-β (R&D Systems). $Bsg^{+/+}$ and $Bsg^{-/-}$ TECs were labeled with calcein-AM beforehand, and then 5.0×10^4 cells/well were added to the upper chamber. The Boyden chamber was incubated for 24 hours at 37°C to allow the possible migration of cells into the lower chamber. The number of migrated cells was estimated as fluorescence using Fluoroskan AscentCF (Labsystems, Helsinki, Finland).

Statistical Analysis

All values are expressed as means ± SD. Statistical analysis was performed with the unpaired, two-tailed Student's *t*-test for single comparisons. Values of $P < 0.05$ were considered to indicate statistically significant differences.

Results

Bsg$^{-/-}$ *Mice Have Less Tubulointerstitial Fibrosis*

To determine the role of Bsg in renal fibrosis, we subjected $Bsg^{+/+}$ and $Bsg^{-/-}$ mice to UUO surgery and compared the degrees of type III collagen deposition in the tubulointerstitium. At 7 days after UUO operation, both genotypes exhibited increased expression of type III collagen on immunohistochemistry (Figure 1A). This deposition became more diffuse and remarkable at 14 days in the interstitium of $Bsg^{+/+}$ mice, whereas $Bsg^{-/-}$ mice showed only a little more fibrosis. Consistent with the immunohistochemical findings, type III collagen mRNA expression also increased at 14 days in $Bsg^{+/+}$ mice compared with $Bsg^{-/-}$ mice, which was revealed by quantitative RT-PCR (Figure 1B).

PAS staining revealed marked tubular dilation and atrophy in both genotypes at 14 days (Figure 1C). It is likely that the infiltration of inflammatory cells was prominent in $Bsg^{+/+}$ mice. To verify the tubular damage, we assessed the number of dilated tubules at 7 and 14 days. There was no significant difference between the two genotypes (Figure 1D), suggesting that both groups operated on had the same extent of renal

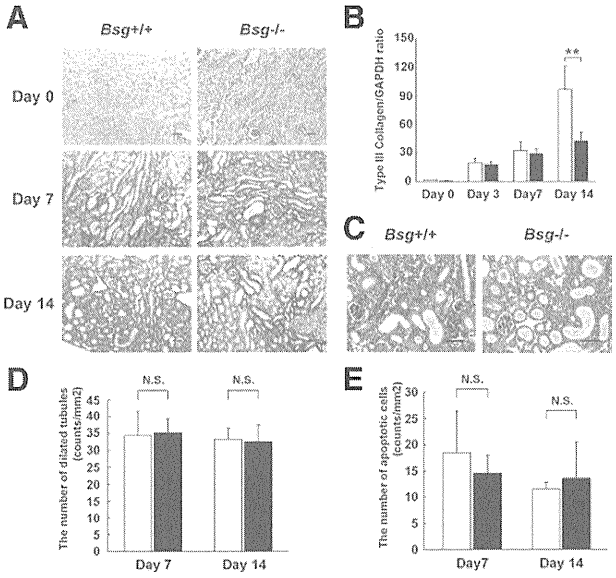

Figure 1. Histological evaluation of the kidneys of $Bsg^{+/+}$ and $Bsg^{-/-}$ mice after UUO. **A:** Type III collagen expression in the tubulointerstitium at 0, 7, and 14 days after UUO operation. Scale bar = 50 μm. **B:** Type III collagen mRNA expression, determined by quantitative reverse transcriptase PCR. Each value was standardized by GAPDH mRNA content as an internal control. Data are means (columns) ± SD (bars); white bar, $Bsg^{+/+}$; black bar, $Bsg^{-/-}$; $^{**}P < 0.01$; $n = 6$. **C:** The tubulointerstitium at 14 days is shown by PAS staining. Scale bar = 50 μm. **D:** The number of dilated tubules (counts/mm^2). Data are means ± SD; white bar, $Bsg^{+/+}$; black bar, $Bsg^{-/-}$; N.S., not significant; $n = 8$. **E:** The number of apoptotic cells (counts/mm^2), assessed by TUNEL assay. Data are means ± SD; white bar, *Bsg+/+*; black bar, $Bsg^{-/-}$; $n = 8$.

damage. We further performed TUNEL assay to examine the effect of Bsg on apoptosis of tubular injuries. But, no obvious difference was observed between the two genotypes (Figure 1E).

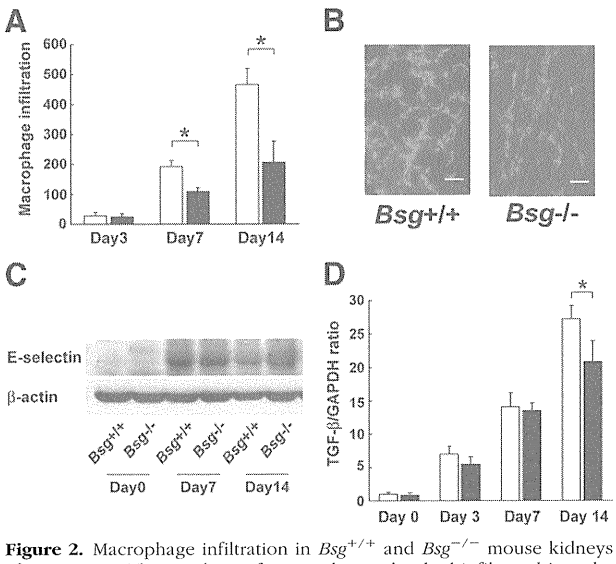

Figure 2. Macrophage infiltration in $Bsg^{+/+}$ and $Bsg^{-/-}$ mouse kidneys after UUO. **A:** The numbers of macrophages that had infiltrated into the tubulointerstitium at 3, 7, and 14 days were counted. Data are means ± SD; white bar, $Bsg^{+/+}$; black bar, $Bsg^{-/-}$; $^{*}P < 0.05$; $n = 6$. **B:** Immunofluorescence staining with F4/80 antibody at 7 days. Scale bar = 50 μm. **C:** Western blotting of E-selectin expression in the kidney after UUO. **D:** TGF-β mRNA, determined by real-time PCR. Each value was standardized by GAPDH mRNA content as an internal control. Data are means ± SD; white bar, $Bsg^{+/+}$; black bar, $Bsg^{-/-}$; $^{*}P < 0.05$; $n = 6$.

Macrophage Infiltration Is Lower in Bsg$^{-/-}$ *Mice*

Macrophage infiltration is a key event for the pathogenesis of renal fibrosis.[42,43] Both $Bsg^{+/+}$ and $Bsg^{-/-}$ mice exhibited only slight macrophage infiltration at day 3 (Figure 2A). Macrophage infiltration into the interstitium became prominent at day 7, and increased more at day 14 (Figure 2, A and B). The infiltrating macrophage number was significantly higher in the $Bsg^{+/+}$ kidneys (Figure 2A).

Macrophage infiltration in the post-obstructed kidney requires adhesion molecules.[44] However, little information about E-selectin is available. Because Bsg acts as an E-selectin ligand on inflammatory cells,[34] we next examined E-selectin expression in the kidney. We found that E-selectin expression was upregulated in the kidney after UUO surgery, but the expression levels were comparable between the genotypes (Figure 2C).

TGF-β serves as a profibrogenic cytokine by directly stimulating the synthesis of extracellular matrix components and indirectly stimulating other profibrogenic factors such as connective tissue growth factor.[45] TGF-β is produced by many types of cells in the UUO model, and

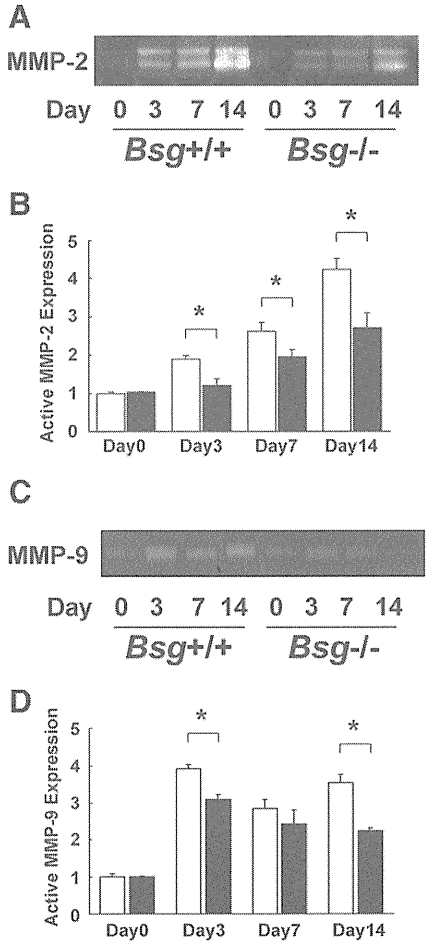

Figure 3. Induction of renal MMPs in the $Bsg^{+/+}$ and $Bsg^{-/-}$ mouse kidneys after UUO. **A:** Zymographic analysis of whole kidney lysates indicating MMP-2 induction. **B:** The intensity of active-MMP-2 bands. Data are means ± SD; white bar, $Bsg^{+/+}$; black bar, $Bsg^{-/-}$; $^{*}P < 0.05$; $n = 6$. **C:** A representative photo of MMP-9 activation in gelatin zymography. **D:** The intensity of active-MMP-9 bands. Data are means ± SD; white bar, $Bsg^{+/+}$; black bar, $Bsg^{-/-}$; $^{*}P < 0.05$; $n = 6$.

macrophage is one of the major sources.[42,45] We found that TGF-β was equally up-regulated in both genotypes until 7 days after UUO surgery (Figure 2D). Then TGF-β expression in $Bsg^{+/+}$ exceeded that in $Bsg^{-/-}$ mice at day 14 (Figure 2D).

MMP-2 and MMP-9 Activities Are Suppressed in Bsg$^{-/-}$ *Mice*

Bsg is known as an inducer of MMP-2 and MMP-9, and they play a key role in maintaining a balance between ECM deposition and degradation. In addition, the increased synthesis of MMPs has been shown to increase in various kidney diseases.[46,47] Therefore, we next investigated MMP activity in the kidney after UUO. Gelatin zymography demonstrated that the activity of MMP-2 was gradually increased, but was always less in $Bsg^{-/-}$ mice: the difference between the genotypes became apparent 3 days after surgery (Figure 3, A and B). On the other hand, the activation of MMP-9 strikingly increased at 3 days after UUO operation in both genotypes, but to lower extents in $Bsg^{-/-}$ mice at 3 days and 14 days (Figure 3, C and D). Their induction remained higher until 14 days in both groups.

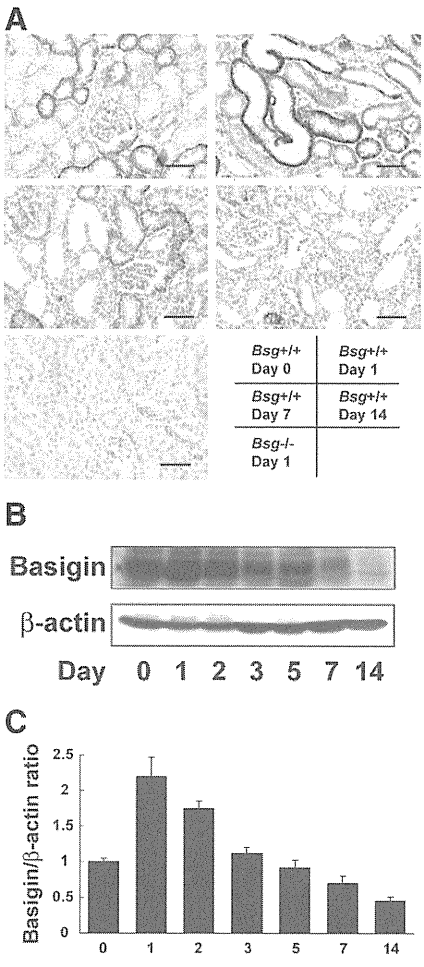

Figure 4. Basigin expression in the UUO model. **A:** Immunohistochemical staining of Bsg in the kidney. Scale bar = 50 μm. **B:** Time course of basigin expression in the UUO model. Bsg protein was determined by Western blotting. **C:** The intensity of Bsg bands was normalized as to β-actin. Data are means ± SD; $^{*}P < 0.05$; $n = 6$.

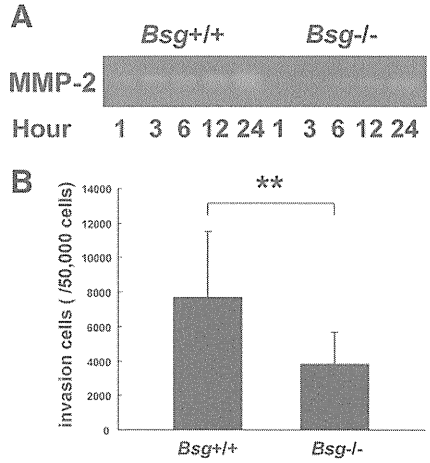

Figure 5. Bsg on TECs contributed to MMP-2 induction and upregulated migration capacity under TGF-β stimuli. **A:** Zymographic analysis indicates MMP-2 production in the culture medium of tubular epithelial cells after TGF-β stimulation. **B:** Migration of tubular epithelial cells was evaluated by cell invasion assay. The number of tubular epithelial cells that had migrated into the lower chamber through basement extract-extracts coated membrane by TGF-β stimulation is indicated. Data are means ± SD; $^{**}P < 0.01$; $n = 30$.

Bsg Expression Is Transiently Upregulated During Acute Phase of Tubulointerstitial Injury

We next examined Bsg expression during the pathogenesis of renal fibrosis. Bsg expression was detected on the basolateral side of the proximal and distal tubules in $Bsg^{+/+}$ mice before UUO operation (Figure 4A), consistent with a previous report.[48] UUO operation transiently and slightly enhanced Bsg expression, reaching the maximum level at day 1 (Figure 4A). However, Bsg expression decreased thereafter, and became very low at day 14 (Figure 4A). Bsg expression was detected in tubular epithelial cells and infiltrating inflammatory cells. The expression reduction was probably attributable to a loss of tubular epithelial cells due to cell death induced by UUO. Western blot data confirmed this observation (Figure 4, B and C). We did not observe any Bsg expression in the kidney of $Bsg^{-/-}$ mice (Figure 4A).

TGF-β Response Is Lower in Primary Bsg$^{-/-}$ *TECs*

Our *in vivo* data showed an apparent association between Bsg and renal fibrosis induced by UUO. To understand the underlying mechanism, we performed *in vitro* experiments. Based on the results shown in Figures 2 and 3, we addressed the effects of Bsg of TECs on MMP-2 production under TGF-β stimulation *in vitro*. When subjected to gelatin zymography, culture media showed that MMP-2 production was indeed induced on TGF-β administration, but the extent of the induction was much lower in $Bsg^{-/-}$ TECs (Figure 5A).

We also examined the invasive capacity of $Bsg^{+/+}$ and $Bsg^{-/-}$ TECs. In the upper chamber, transwell mem-

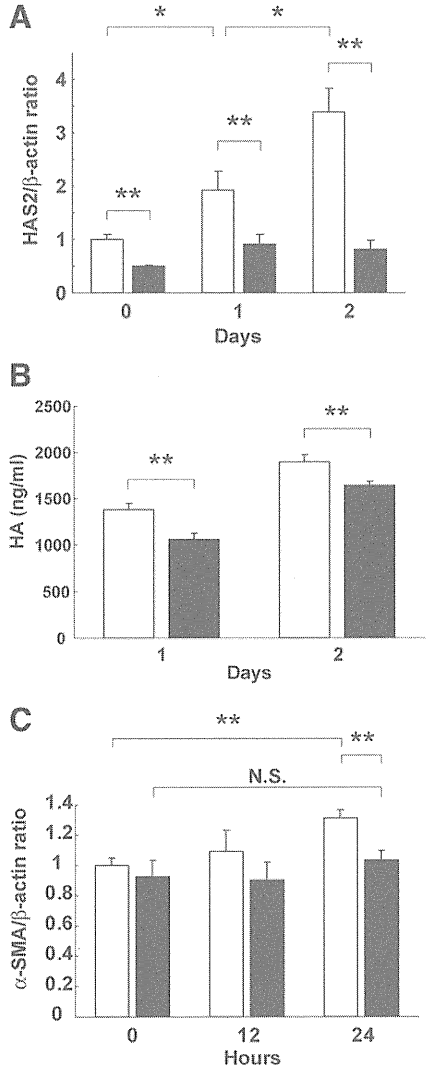

Figure 6. Bsg promoted hyaluronan synthesis and was related to α-SMA induction. **A:** Hyaluronic acid synthase 2 (HAS2) mRNA determined by real-time PCR in MEF under TGF-β stimulation. Each value was standardized by β-actin mRNA content as an internal control. Data are means ± SD; white bar, $Bsg^{+/+}$; black bar, $Bsg^{-/-}$; $^{*}P < 0.05$; $^{**}P < 0.01$; $n = 3$. **B:** Hyaluronan (HA) production in MEF under TGF-β stimulation. White bar, $Bsg^{+/+}$; black bar, $Bsg^{-/-}$; $^{**}P < 0.01$. **C:** α-SMA mRNA determined by real-time PCR in MEF under TGF-β stimuli. Each value was standardized by β-actin mRNA content as an internal control. Data are means ± SD; white bar, $Bsg^{+/+}$; black bar, $Bsg^{-/-}$; $^{**}P < 0.01$; N.S., not significant; $n = 3$.

branes were coated with basement membrane extract, and then TECs were seeded on the membrane. TGF-β was added in the lower chamber. As shown in Figure 5B, $Bsg^{-/-}$ TECs exhibited a lower ability to transmigrate.

Bsg Contributes to Hyaluronan Synthesis on TGF-β Stimulation

Because it has been reported that Bsg promotes hyaluronan production in tumor cells and fibroblasts,[23–25,49] we asked whether or not Bsg deficiency would affect hyaluronan production by MEF. We found that the expression of hyaluronic acid synthase 2, which biosynthesizes hyaluronan, was lower in $Bsg^{-/-}$ MEF even in the steady state (Figure 6A). Furthermore, TGF-β enhanced hyaluronic acid synthase 2 expression in $Bsg^{+/+}$ MEF, but not in $Bsg^{-/-}$ MEF (Figure 6A). We also found the α-SMA mRNA level was elevated 24 hours after TGF-β stimulation in $Bsg^{+/+}$ MEF, but not in $Bsg^{-/-}$ MEF (Figure 6C). This result was in line with recent reports that endogenous hyaluronan promotes α-SMA expression in fibroblast.[10,11]

Discussion

Our *in vivo* data showed that $Bsg^{-/-}$ mice had much less fibrosis, and the difference between the genotypes became apparent 14 days after UUO surgery. MMP-2 and MMP-9 activations were enhanced in both genotypes, but the extent was significantly less in $Bsg^{-/-}$ mice—the difference became apparent as early as 3 days after UUO operation. *In vitro* experiments demonstrated that Bsg on TECs promoted active MMP-2 production in response to TGF-β, and that Bsg on fibroblasts played a critic al role in hyaluronan production in response to TGF-β. Because TGF-β expression was upregulated after UUO to similar extents in $Bsg^{+/+}$ and $Bsg^{-/-}$ mice up to day 7, it is conceivable that the responsiveness to TGF-β is linked to the difference in renal fibrosis in $Bsg^{+/+}$ and $Bsg^{-/-}$ mice. In this context, it is noteworthy that both MMP-2 and MMP-9 are an activator of TGF-β,[4,5] and that Bsg is a strong inducer of MMP family. Thus, there may be a molecular circuit between Bsg, MMPs, and TGF-β (Figure 7). Taken together, our results established that Bsg is an important regulator of renal fibrosis.

UUO is a well-characterized model of renal injury leading to renal fibrosis.[43,50] A number of studies have revealed major pathways leading to the development of renal fibrosis after UUO surgery: the initial event is interstitial infiltration of macrophages that produce cytokines responsible for fibroblast proliferation and activation. After UUO operation, macrophages infiltrate the tubulointerstitial space from blood vessels and become a major source of cytokines, such as TGF-β. Macrophage infiltration was more prominent in $Bsg^{+/+}$ kidneys, and its time course was consistent with the pathogenesis profile of renal fibrosis. It is known that macrophages express Bsg, and that Bsg could be a ligand for E-selectin.[27,34] We also confirmed that Bsg on THP-1, the human monocytic cell line, bound to E-selectin (data not shown). Consider-

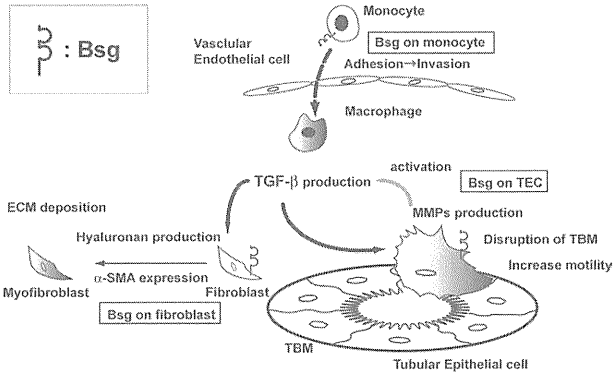

Figure 7. Schematic diagram showing the possible contribution of Bsg to renal fibrosis after UUO.

ing that E-selectin expression was induced to similar degrees in both genotypes, it is likely that the difference in macrophage infiltration between $Bsg^{+/+}$ and $Bsg^{-/-}$ mice is due to the presence of Bsg on macrophages. Indeed, it was reported that mice with triple knockout of E-, P-, and L-selectin show a marked reduction in macrophage infiltration into the obstructed kidney, and are protected from fibrosis in UUO.[51] Thus, macrophage infiltration could be the primary cause of renal fibrosis after UUO, and could cause the difference between $Bsg^{+/+}$ and $Bsg^{-/-}$ mice. In the current study, however, macrophage infiltration began 7 days after surgery, when MMP-2 expression had already been induced (starting from day 3, when TGF-β expression induction was also observed). Therefore, macrophage infiltration cannot fully explain the Bsg involvement with renal fibrosis. Moreover, TGF-β expression was induced to similar extents until 7 days in both genotypes. Our *in vitro* study demonstrated the genotype-dependent responsiveness to TGF-β in TECs and fibroblasts. Together, it is likely that both the Bsg-mediated migration of macrophages and the genotype-dependent responsiveness to TGF-β could be important to the formation of the genotype-dependent difference of renal fibrosis after UUO.

Phenotypic transition of resident renal cells into myofibroblasts is observed in a UUO model. TECs are one of them. Currently, the degree to which this process contributes to kidney fibrosis remains a matter of intense debate.[52,53] Tubular basement membrane regulates numerous cell-matrix interactions that are pivotal to the maintenance of the epithelial phenotype. In the process of renal fibrosis, MMPs are an important factor for the disruption of tubular basement membrane.[54,55] As a result, TECs lose their polarity and acquire contractile motility.[55] Considering that TECs have a TGF-β receptor and produce MMP-2 and MMP-9 on TGF-β stimulation,[56] our data suggest that Bsg on TECs (an inducer of both MMP-2 and MMP-9) is at least partly responsible for disrupting tubular basement membrane and matrix remodeling by MMP induction.

Resident fibroblasts could also be the source of myofibroblasts.[42] Generally, the wound repair process is characterized by the activation of quiescent fibroblasts and their differentiation into myofibroblasts.[30] Hyaluronan promotes α-SMA expression in fibroblasts and orchestrates TGF-β-dependent maintenance of the myofibroblast phenotype.[10,11] Little is known about the precise mechanism underlying how hyaluronan induces α-SMA in fibroblasts, but it is assumed that the hyaluronan macromolecular assembly in the pericellular environment contributes to mediate various signaling.[10] Previous reports and the present study have demonstrated that Bsg promotes hyaluronan production and subsequent α-SMA expression in fibroblasts.[25,49]

In summary, Bsg is a multifunctional molecule engaged in hyaluronan production, MMP production, cell adhesion, and α-SMA induction in renal fibrosis. Intervention targeting Bsg would have multiple effects on the prevention of renal fibrosis.

Acknowledgments

We thank Norihiko Suzuki, Naoko Asano, and Yuriko Sawa for their excellent technical assistance and Hitomi Aoyama for secretarial assistance.

References

1. Schainuck LI, Striker GE, Cutler RE, Benditt EP: Structural-functional correlations in renal disease. II. The correlations. Hum Pathol 1970, 1:631–641
2. Gabbiani G: The myofibroblast in wound healing and fibrocontractive diseases. J Pathol 2003, 200:500–503
3. Mauviel A, Chung KY, Agarwal A, Tamai K, Uitto J: Cell-specific induction of distinct oncogenes of the Jun family is responsible for differential regulation of collagenase gene expression by transforming growth factor-beta in fibroblasts and keratinocytes. J Biol Chem 1996, 271:10917–10923
4. Philipp K, Riedel F, Germann G, Hormann K, Sauerbier M: TGF-beta antisense oligonucleotides reduce mRNA expression of matrix metalloproteinases in cultured wound-healing-related cells. Int J Mol Med 2005, 15:299–303
5. Karsdal MA, Larsen L, Engsig MT, Lou H, Ferreras M, Lochter A, Delaisse JM, Foged NT: Matrix metalloproteinase-dependent activation of latent transforming growth factor-beta controls the conversion of osteoblasts into osteocytes by blocking osteoblast apoptosis. J Biol Chem 2002, 277:44061–44067
6. Yu Q, Stamenkovic I: Cell surface-localized matrix metalloproteinase-9 proteolytically activates TGF-beta and promotes tumor invasion and angiogenesis. Genes Dev 2000, 14:163–176
7. Jenkins RH, Thomas GJ, Williams JD, Steadman R: Myofibroblastic differentiation leads to hyaluronan accumulation through reduced hyaluronan turnover. J Biol Chem 2004, 279:41453–41460
8. Meran S, Thomas D, Stephens P, Martin J, Bowen T, Phillips A, Steadman R: Involvement of hyaluronan in regulation of fibroblast phenotype. J Biol Chem 2007, 282:25687–25697
9. Meran S, Thomas DW, Stephens P, Enoch S, Martin J, Steadman R, Phillips AO: Hyaluronan facilitates transforming growth factor-beta1-mediated fibroblast proliferation. J Biol Chem 2008, 283:6530–6545
10. Webber J, Jenkins RH, Meran S, Phillips A, Steadman R: Modulation of TGFbeta1-dependent myofibroblast differentiation by hyaluronan. Am J Pathol 2009, 175:148–160
11. Webber J, Meran S, Steadman R, Phillips A: Hyaluronan orchestrates transforming growth factor-beta1-dependent maintenance of myofibroblast phenotype. J Biol Chem 2009, 284:9083–9092
12. Biswas C: Tumor cell stimulation of collagenase production by fibroblasts. Biochem Biophys Res Commun 1982, 109:1026–1034
13. Yurchenko V, Constant S, Bukrinsky M: Dealing with the family: cD147 interactions with cyclophilins. Immunology 2006, 117:301–309
14. Biswas C, Zhang Y, DeCastro R, Guo H, Nakamura T, Kataoka H, Nabeshima K: The human tumor cell-derived collagenase stimulatory factor (renamed EMMPRIN) is a member of the immunoglobulin superfamily. Cancer Res 1995, 55:434–439
15. Riethdorf S, Reimers N, Assmann V, Kornfeld JW, Terracciano L, Sauter G, Pantel K: High incidence of EMMPRIN expression in human tumors. Int J Cancer 2006, 119:1800–1810
16. Schneiderhan W, Scheler M, Holzmann KH, Marx M, Gschwend JE, Bucholz M, Gress TM, Seufferlein T, Adler G, Oswald F: CD147 silencing inhibits lactate transport and reduces malignant potential of pancreatic cancer cells in in vivo and in vitro models. Gut 2009, 58:1391–1398
17. Slomiany MG, Grass GD, Robertson AD, Yang XY, Maria BL, Beeson C, Toole BP: Hyaluronan. CD44, and EMMPRIN regulate lactate efflux and membrane localization of monocarboxylate transporters in human breast carcinoma cells. Cancer Res 2009, 69:1293–1301
18. Chen X, Lin J, Kanekura T, Su J, Lin W, Xie H, Wu Y, Li J, Chen M, Chang J: A small interfering CD147-targeting RNA inhibited the proliferation, invasiveness, and metastatic activity of malignant melanoma. Cancer Res 2006, 66:11323–11330
19. Su J, Chen X, Kanekura T: A CD147-targeting siRNA inhibits the proliferation, invasiveness, and VEGF production of human malignant

melanoma cells by down-regulating glycolysis. Cancer Lett 2009, 273:140–147
20. Tang Y, Kesavan P, Nakada MT, Yan L: Tumor-stroma interaction: positive feedback regulation of extracellular matrix metalloproteinase inducer (EMMPRIN) expression and matrix metalloproteinase-dependent generation of soluble EMMPRIN. Mol Cancer Res 2004, 2:73–80
21. Tang Y, Nakada MT, Kesavan P, McCabe F, Millar H, Rafferty P, Bugelski P, Yan L: Extracellular matrix metalloproteinase inducer stimulates tumor angiogenesis by elevating vascular endothelial cell growth factor and matrix metalloproteinases. Cancer Res 2005, 65: 3193–3199
22. Tang Y, Nakada MT, Rafferty P, Laraio J, McCabe FL, Millar H, Cunningham M, Snyder LA, Bugelski P, Yan L: Regulation of vascular endothelial growth factor expression by EMMPRIN via the PI3K-Akt signaling pathway. Mol Cancer Res 2006, 4:371–377
23. Misra S, Ghatak S, Zoltan-Jones A, Toole BP: Regulation of multidrug resistance in cancer cells by hyaluronan. J Biol Chem 2003, 278: 25285–25288
24. Marieb EA, Zoltan-Jones A, Li R, Misra S, Ghatak S, Cao J, Zucker S, Toole BP: Emmprin promotes anchorage-independent growth in human mammary carcinoma cells by stimulating hyaluronan production. Cancer Res 2004, 64:1229–1232
25. Toole BP: Hyaluronan: from extracellular glue to pericellular cue. Nat Rev Cancer 2004, 4:528–539
26. Tang W, Chang SB, Hemler ME: Links between CD147 function, glycosylation, and caveolin-1. Mol Biol Cell 2004, 15:4043–4050
27. Arora K, Gwinn WM, Bower MA, Watson A, Okwumabua I, MacDonald HR, Bukrinsky MI, Constant SL: Extracellular cyclophilins contribute to the regulation of inflammatory responses. J Immunol 2005, 175:517–522
28. Kirk P, Wilson MC, Heddle C, Brown MH, Barclay AN, Halestrap AP: CD147 is tightly associated with lactate transporters MCT1 and MCT4 and facilitates their cell surface expression. EMBO J 2000, 19:3896–3904
29. Philp NJ, Wang D, Yoon H, Hjelmeland LM: Polarized expression of monocarboxylate transporters in human retinal pigment epithelium and ARPE-19 cells. Invest Ophthalmol Vis Sci 2003, 44:1716–1721
30. Huet E, Vallee B, Szul D, Verrecchia F, Mourah S, Jester JV, Hoang-Xuan T, Menashi S, Gabison EE: Extracellular matrix metalloproteinase inducer/CD147 promotes myofibroblast differentiation by inducing alpha-smooth muscle actin expression and collagen gel contraction: implications in tissue remodeling. FASEB J 2008, 22: 1144–1154
31. Igakura T, Kadomatsu K, Kaname T, Muramatsu H, Fan QW, Miyauchi T, Toyama Y, Kuno N, Yuasa S, Takahashi M, Senda T, Taguchi O, Yamamura K, Arimura K, Muramatsu T: A null mutation in basigin, an immunoglobulin superfamily member, indicates its important roles in peri-implantation development and spermatogenesis. Dev Biol 1998, 194:152–165
32. Igakura T, Kadomatsu K, Taguchi O, Muramatsu H, Kaname T, Miyauchi T, Yamamura K, Arimura K, Muramatsu T: Roles of basigin, a member of the immunoglobulin superfamily, in behavior as to an irritating odor, lymphocyte response, and blood-brain barrier. Biochem Biophys Res Commun 1996, 224:33–36
33. Naruhashi K, Kadomatsu K, Igakura T, Fan QW, Kuno N, Muramatsu H, Miyauchi T, Hasegawa T, Itoh A, Muramatsu T, Nabeshima T: Abnormalities of sensory and memory functions in mice lacking Bsg gene. Biochem Biophys Res Commun 1997, 236:733–737
34. Kato N, Yuzawa Y, Kosugi T, Hobo A, Sato W, Miwa Y, Sakamoto K, Matsuo S, Kadomatsu K: The E-selectin ligand basigin/CD147 is responsible for neutrophil recruitment in renal ischemia/reperfusion. J Am Soc Nephrol 2009, 20:1565–1576
35. Chen S, Kadomatsu K, Kondo M, Toyama Y, Toshimori K, Ueno S, Miyake Y, Muramatsu T: Effects of flanking genes on the phenotypes of mice deficient in basigin/CD147. Biochem Biophys Res Commun 2004, 324:147–153
36. Nomura A, Nishikawa K, Yuzawa Y, Okada H, Morgan BP, Piddlesden SJ, Nadai M, Hasegawa T, Matsuo S: Tubulointestinal injury induced in rats by a monoclonal antibody that inhibits function of membrane inhibitor of complement. J Clin Invest 1995, 96:2348–2356
37. Kadomatsu K, Hagihara M, Akhter S, Fan QW, Muramatsu H, Muramatsu T: Midkine induces the transformation of NIH3T3 cells. Br J Cancer 1997, 75:354–359
38. Kosugi T, Yuzawa Y, Sato W, Arata-Kawai H, Suzuki N, Kato N, Matsuo S, Kadomatsu K: Midkine is involved in tubulointerstitial inflammation associated with diabetic nephropathy. Lab Invest 2007, 87:903–913
39. Camussi G, Brentijens JR, Noble B, Kerjaschiki D, Malavasi F, Roholt OA, Farquhar MG, Andres G: Antibody-induced redistribution of Hymann antigen on the surface of cultured glomerular visceral epithelial cells: possible role in the pathogenesis of Hymann glomerulonephritis. J Immunol 1985, 135:2409–2416
40. Tsuboi N, Yoshikai Y, Matsuo S, Kikuchi T, Iwami K, Nagai Y, Takeuchi O, Akira S, Matsuguchi T: Roles of toll-like receptors in C-C chemokine production by renal epithelial cells. J Immunol 2002, 169:2026–2033
41. Nguyen A, Burack WR, Stock JL, Kortum R, Chaika OV, Afkarian M, Muller WJ, Murphy KM, Morrison DK, Lewis RE, McNeish J, Shaw AS: Kinase suppressor of Ras (KSR) is a scaffold which facilitates mitogen-activated protein kinase activation in vivo. Mol Cell Biol 2002, 22:3035–3045
42. Chevalier RL, Forbes MS, Thornhill BA: Ureteral obstruction as a model of renal interstitial fibrosis and obstructive nephropathy. Kidney Int 2009, 75:1145–1152
43. Bascands JL, Schanstra JP: Obstructive nephropathy: insights from genetically engineered animals. Kidney Int 2005, 68:925–937
44. Rouschop KM, Sewnath ME, Claessen N, Roelofs JJ, Hoedemaeker I, van der Neut R, Aten J, Pals ST, Weening JJ, Florquin S: CD44 deficiency increases tubular damage but reduces renal fibrosis in obstructive nephropathy. J Am Soc Nephrol 2004, 15:674–686
45. Wolf G: Renal injury due to renin-angiotensin-aldosterone system activation of the transforming growth factor-beta pathway. Kidney Int 2006, 70:1914–1919
46. Steinmann-Niggli K, Ziswiler R, Kung M, Marti HP: Inhibition of matrix metalloproteinases attenuates anti-Thy1.1 nephritis. J Am Soc Nephrol 1998, 9:397–407
47. Marti HP, McNeil L, Thomas G, Davies M, Lovett DH: Molecular characterization of a low-molecular-mass matrix metalloproteinase secreted by glomerular mesangial cells as PUMP-1. Biochem J 1992, 285(Pt 3):899–905
48. Deora AA, Philp N, Hu J, Bok D, Rodriguez-Boulan E: Mechanisms regulating tissue-specific polarity of monocarboxylate transporters and their chaperone CD147 in kidney and retinal epithelia. Proc Natl Acad Sci U S A 2005, 102:16245–16250
49. Toole BP, Slomiany MG: Hyaluronan. CD44 and Emmprin: partners in cancer cell chemoresistance. Drug Resist Updat 2008, 11:110–121
50. Klahr S, Morrissey J: Obstructive nephropathy and renal fibrosis. Am J Physiol Renal Physiol 2002, 283:F861–875
51. Lange-Sperandio B, Cachat F, Thornhill BA, Chevalier RL: Selectins mediate macrophage infiltration in obstructive nephropathy in newborn mice. Kidney Int 2002, 61:516–524
52. Lin SL, Kisseleva T, Brenner DA, Duffield JS: Pericytes and perivascular fibroblasts are the primary source of collagen-producing cells in obstructive fibrosis of the kidney. Am J Pathol 2008, 173:1617–1627
53. Liu Y: New insights into epithelial-mesenchymal transition in kidney fibrosis. J Am Soc Nephrol 2010, 21:212–222
54. Zavadil J, Bottinger EP: TGF-beta and epithelial-to-mesenchymal transitions. Oncogene 2005, 24:5764–5774
55. Zeisberg M, Maeshima Y, Mosterman B, Kalluri R: Renal fibrosis. Extracellular matrix microenvironment regulates migratory behavior of activated tubular epithelial cells. Am J Pathol 2002, 160:2001–2008
56. Yang J, Liu Y: Dissection of key events in tubular epithelial to myofibroblast transition and its implications in renal interstitial fibrosis. Am J Pathol 2001, 159:1465–1475

Clin Exp Nephrol (2011) 15:346–354
DOI 10.1007/s10157-011-0408-2

ORIGINAL ARTICLE

Growth factor Midkine is involved in the pathogenesis of renal injury induced by protein overload containing endotoxin

Kiyonari Kato · Tomoki Kosugi · Waichi Sato · Hanayo Arata-Kawai · Takenori Ozaki · Naotake Tsuboi · Isao Ito · Hideo Tawada · Yukio Yuzawa · Seiichi Matsuo · Kenji Kadomatsu · Shoichi Maruyama

Received: 5 August 2010 / Accepted: 6 January 2011 / Published online: 1 March 2011

Abstract

Background Growth factor Midkine (MK), which expresses on endothelial cells and renal proximal tubules, has been implicated in inflammation-related kidney diseases such as ischemic reperfusion-induced tubulointerstitial injury and diabetic nephropathy. The biological actions of MK are elicited through its chemotactic activity and chemokine-driven inflammatory pathway. Post-infectious glomerulonephritis is caused by the deposition of immune complexes into glomeruli by infiltrating a number of inflammatory cells. Therefore, we investigated whether MK might be involved in the pathogenesis of acute glomerulonephritis.

Methods We induced endocapillary proliferative glomerulonephritis in 129/SV mice using intraperitoneal injections of a large amount of protein.

Results In contrast to mice deficient in MK ($Mdk^{-/-}$), $Mdk^{+/+}$ mice induced by protein overload demonstrated more diffuse cellular proliferation in the mesangial areas and capillary lumens, eventually leading to glomerular damage and tubulointerstitial injury. This pathological observation could be attributable to neutrophil infiltration through the chemotaxis and stimulation of the MK-macrophage inflammatory protein (MIP)-2 pathway, but appeared to be due to the MK-related immunoglobulin (Ig)G deposition and C3 activation. These findings are often seen in infectious-related glomerular injury. Furthermore, the profile of MK expression was strongly consistent with that of glomerular damage and tubulointersititial injury.

Conclusion This study might provide a new insight into understanding the deleterious role of MK in endocapillary proliferative glomerulonephritis induced by protein overload.

Keywords Midkine · Protein-overload mouse model · Endocapillary proliferative glomerulonephritis

Electronic supplementary material The online version of this article (doi:10.1007/s10157-011-0408-2) contains supplementary material, which is available to authorized users.

K. Kato · T. Kosugi · W. Sato (✉) · H. Arata-Kawai · T. Ozaki · N. Tsuboi · I. Ito · Y. Yuzawa · S. Matsuo · S. Maruyama
Division of Nephrology, Nagoya University Graduate School of Medicine, 65 Tsurumai, Showa-ku, Nagoya, Aichi 466-8550, Japan
e-mail: waichi@med.nagoya-u.ac.jp

H. Tawada
Tawada Clinic, 2-15-23 Kaminagoya Nishi-ku, Nagoya, Aichi 451-0025, Japan

K. Kadomatsu
Division of Biochemistry, Nagoya University Graduate School of Medicine, 65 Tsurumai, Showa-ku, Nagoya, Aichi 466-8550, Japan

Introduction

Glomerular injury is one of the most important parameters for predicting renal outcome in various forms of acute progressive renal injury. This key event, which occurs either as primary glomerular disease or as a part of the process of various systemic diseases, accompanies immune-mediated mechanisms such as the cytokine-driven inflammatory system and immune complex formation [1]. In particular, glomerular endothelial dysfunction, which is caused by an infectious inflammation and an increase of the capillary pressure leading to the promotion of glomerular permeability, results in the filtration of excessive amounts

of protein into the lumen of the proximal tubules [2, 3]. Reabsorption of the filtered protein activates the tubular epithelium to generate inflammatory substances including chemokines, which are secreted into the basolateral side of the tubules, instigating a tubulointerstitial inflammatory reaction [3].

Midkine (MK), which is a heparin-binding growth factor, has been implicated in neuronal survival and differentiation, and cancer development [4]. For kidney disease, MK is involved in the pathogenesis of inflammation-related diseases including ischemic reperfusion-induced tubulointerstitial injury [5], cisplatin-induced chronic tubulointerstitial damage [6] and streptozotocin-induced diabetic nephropathy [7, 8]. The biological actions of MK are elicited through its chemotactic activity and chemokine-driven inflammatory pathway; however, the critical role of MK in acute glomerulonephritis has not yet been elucidated. Streptococcal glomerulonephritis is caused by the deposition of infectious immune complexes into glomeruli, resulting from combining bacteria-derived antigens with human-derived antibodies. Light microscopy demonstrates diffuse endocapillary hypercellularity due to the infiltration of neutrophils and macrophages, as well as the proliferation of mesangial cells and endothelial cells. In this study, we caused severe IgG and C3 depositions in glomeruli by the administration of a large amount of different species-derived protein and promoted the influx of inflammatory cells in glomeruli by endotoxin. Pathophysiologically, this model would appear to be infectious glomerular injury such as human acute poststreptococcal glomerulonephritis. Based on our emerging data, we investigated in the present study whether MK might be involved in the pathogenesis of the acute glomerulonephritis induced by protein overload containing endotoxin.

Materials and methods

Animals and experimental design

Mice deficient in the MK gene (*Mdk*) were generated as described previously [9]. After backcrossing of $Mdk^{+/-}$ mice for 18 generations with 129/SV mice, $Mdk^{+/-}$ mice were mated with each other to generate $Mdk^{+/+}$ and $Mdk^{-/-}$ mice to use in this study. Experiments were performed on 8–12-week-old female mice weighing 20–25 g that were housed under controlled environmental conditions and maintained with standard food and water. $Mdk^{+/+}$ and $Mdk^{-/-}$ mice ($n = 8$ in each group) were treated with consecutive daily intraperitoneal injections of bovine serum albumin (BSA; catalog no. A-4503, Sigma–Aldrich, St. Louis, MO, USA) solution (10 mg/g body weight per day) for 14 days (Fig. 1A). Mice were sacrificed to obtain the kidneys and blood at 7, 14 and 28 days after the BSA administration. Blood urea nitrogen (BUN), urinary protein and creatinine were measured using a Iatrochrom UN kit (Iatron Co., Ltd., Tokyo, Japan), a micro-TP test kit (Wako, Osaka, Japan) and a Cre-Kainos kit (Kainos Co., Ltd., Tokyo, Japan), respectively [7]. The kidney tissues were processed for histology, protein and mRNA extraction. All animal experiments were performed in accordance with the animal experimentation guide of Nagoya University Graduate School of Medicine.

Renal histology

Kidneys were fixed in 4% paraformaldehyde, embedded in paraffin, sectioned at 2 μm thickness before periodic

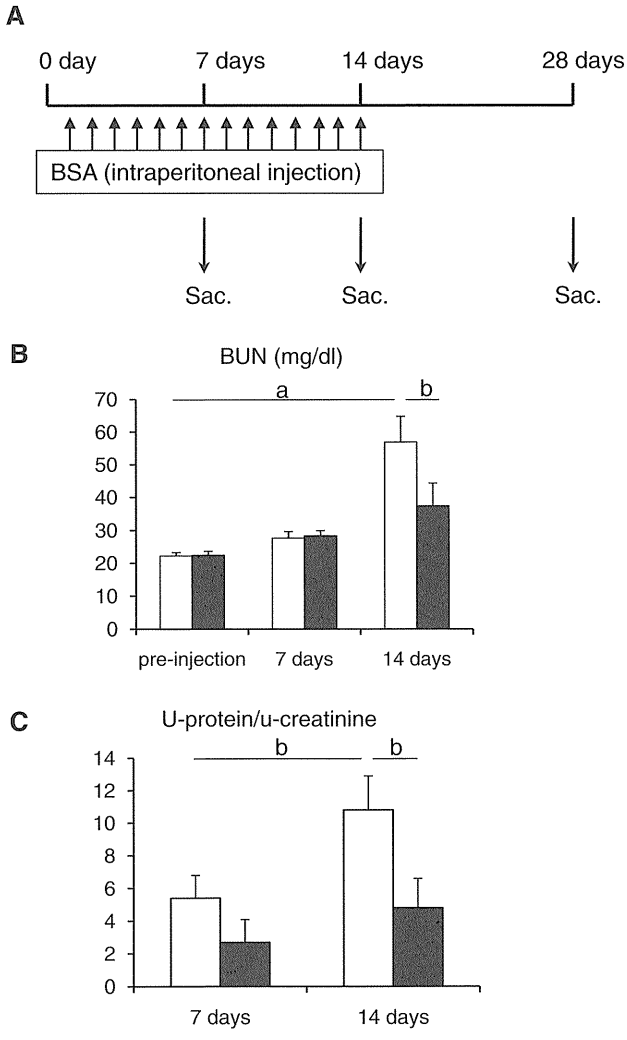

Fig. 1 Experimental design and renal function. Experimental design (**A**), BUN level (**B**) and urinary protein to urinary creatinine ratio (**C**) are shown. *Sac.* sacrifice. Data are shown as the mean (*columns*) and SD (*bars*). *White columns*, $Mdk^{+/+}$ mice; *black columns*, $Mdk^{-/-}$ mice. *a* $p < 0.01$, *b* $p < 0.05$. $n = 8$ in each group

acid-Schiff (PAS) staining. The sections were analyzed to evaluate glomerular and tubulointerstitial injuries in each region by light microscopy. The extent of glomerular injury including mesangial expansion, endocapillary cell proliferation and narrowing of the capillary lumen, was assessed by examining 40 glomeruli cut at their vascular pole in a section, using semiquantitative score method (grades 0 to +4: grade 0, no injury of a glomerulus; grade 1, injury of up to 25% of a glomerulus; grade 2, injury of 25–50% of a glomerulus; grade 3, injury of 50–75% of a glomerulus; grade 4, injury of 75–100% of a glomerulus). For analysis of the tubulointerstitium, the degree of tubular injury (i.e., cast formation, tubular dilation, detachment of tubular epithelial cells and condensation of tubular nuclei) was assessed by semiquantitative score method (grades 0 to +4) in all fields of the cortex for each section as described previously: grade 0, no injury of tubules; grade 1, injury of up to 25% of tubules; grade 2, injury of 25–50% of tubules; grade 3, injury of 50–75% of tubules; grade 4, injury of 75–100% of tubules [10].

The sections embedded in paraffin were also incubated with a goat anti-human MK antibody, followed by detection with biotin-conjugated rabbit anti-goat IgG (Nichirei, Tokyo, Japan). Immnunostaining was performed by the streptavidin–biotin immunoperoxidase method (Chemicon International, Temecula, CA, USA). The staining was visualized with 3,3′-diaminobenzidine (Dako, Carpinteria, CA, USA), a brown color being produced [8].

Another tissue sample was embedded in OCT compound and frozen in liquid nitrogen for immunostaining. Sections were cut at 4 μm with a cryostat and fixed in acetone. The cryosections were stained with FITC-rabbit anti-mouse IgG antibody (Invitrogen, Camarillo, CA, USA) and FITC-goat anti-mouse C3 antibody (ICN Pharmaceuticals Inc., Aurora, OH, USA). The cryosections were also stained with a monoclonal rat anti-mouse neutrophil marker 7/4 (Serotec Ltd., Oxford, UK), followed by detection of depositions with FITC-rabbit anti-rat IgG (Zymed Laboratories, Inc., South San Francisco, CA, USA). Leukocytes positive for the 7/4 were counted by examining 40 glomeruli and 20 fields of the cortex under a microscope at ×400 magnification in a blind manner by two independent observers. Negative controls were performed by the replacement of primary antibodies with species-matched antibodies.

Electron microscopy

Kidneys at 28 days were fixed in glutaraldehyde, post-fixed with osmium tetraoxide, and embedded in Epon 812 (Nisshin EM Co., Tokyo, Japan). The ultrathin sections were examined with a H7100 electron microscope (Hitachi Co. Ltd., Ibaraki, Japan).

Western blot analysis

Mouse kidney tissues were snap-frozen in liquid nitrogen for protein isolation. Western blot analysis was performed as described previously [8]. The blots were subsequently incubated with a rabbit anti-MK antibody or a mouse monoclonal anti-β-actin antibody (Sigma–Aldrich), followed by incubation with peroxidase-conjugated rabbit IgG or mouse IgG (Jackson Immunoresearch Laboratories Inc., West Grove, PA, USA). For evaluation of IgG expression, the blots were incubated only with peroxidase-conjugated rabbit IgG (Jackson Immunoresearch Laboratories Inc.) Proteins were visualized with an enhanced chemiluminescence detection system (Amersham Pharmacia, Piscataway NJ, USA). The density of each band was determined using the public domain NIH Image J program.

Northern blot analysis

Mouse kidney tissues were snap-frozen in liquid nitrogen for total mRNA isolation, as described previously [8]. To standardize the Northern blots, we used a housekeeping gene, glyceraldehyde-3-phosphate dehydrogenase (*GAPDH*), as an internal control. Chemokine expressions including those of MIP-2, monocyte chemoattractant protein (MCP)-1 and transforming growth factor (TGF)-β_1, were assessed.

Statistical analysis

All values are expressed as means ± SD. Statistical analysis was performed with an unpaired, two-tailed student *t* test for single comparisons or analysis of variance with a post-hoc test using Tukey's method for multiple comparisons. A p value of <0.05 was considered to indicate a significant difference.

Results

Renal injury is less marked in MK-deficient mice

Renal function was evaluated by means of BUN values. Neither $Mdk^{+/+}$ nor $Mdk^{-/-}$ mice altered BUN levels at 7 days after treatment, but those of $Mdk^{+/+}$ mice strikingly increased at 14 days (Fig. 1B). Both groups showed a marked rise of proteinuria at 7 days, which was significantly more severe in $Mdk^{+/+}$ than in $Mdk^{-/-}$ mice at 14 days (Fig. 1C). We then compared the degrees of both glomerular and tubulointerstitial injuries in $Mdk^{+/+}$ and $Mdk^{-/-}$ mice. $Mdk^{-/-}$ mice displayed mild glomerular damage at 14 days after treatment, whereas $Mdk^{+/+}$ mice showed more diffuse, global and severe cellular proliferation such as mesangial

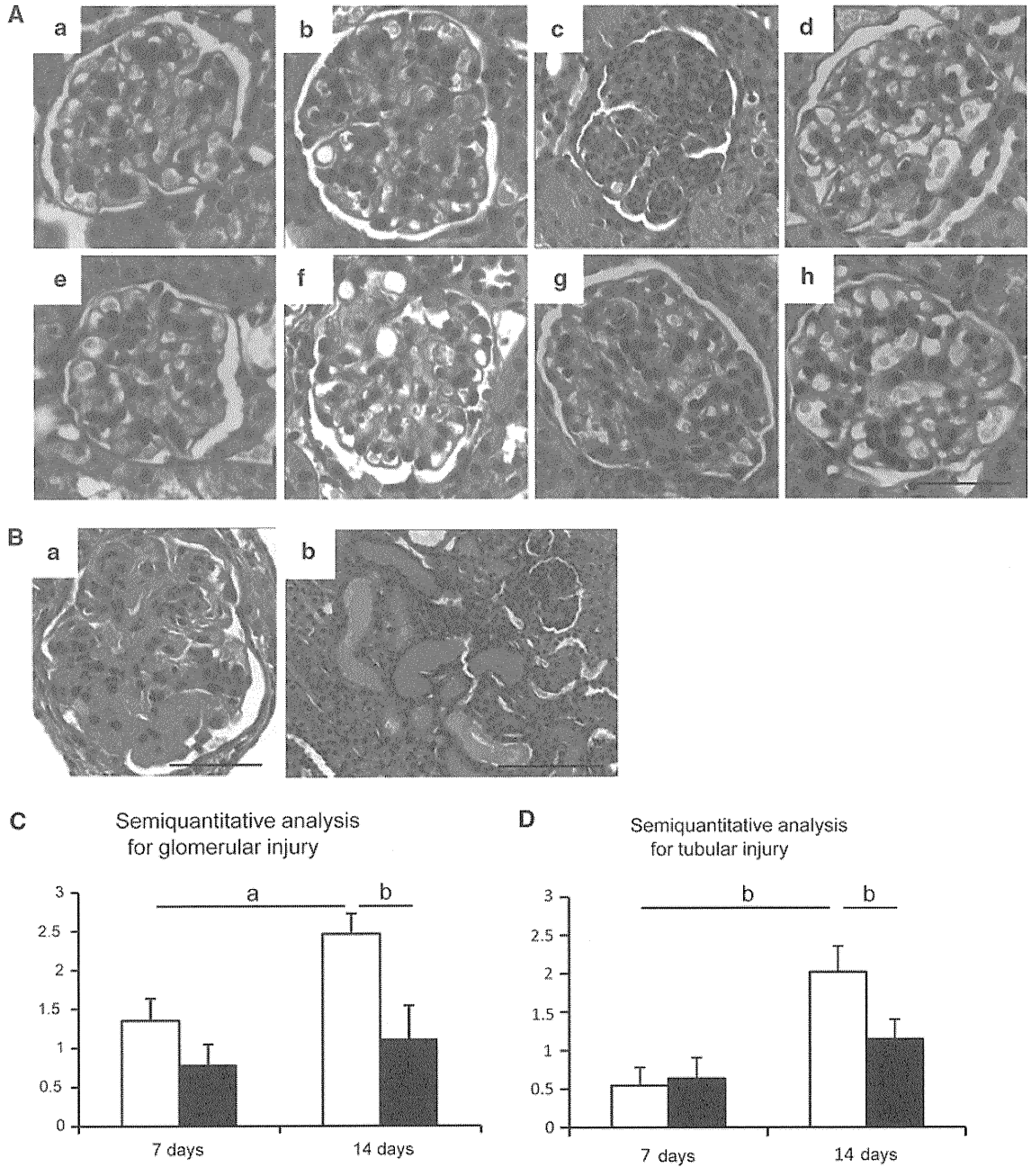

Fig. 2 Renal histology in protein-overload $Mdk^{+/+}$ and $Mdk^{-/-}$ mice. **A** The glomerulus at 0, 7, 14 and 28 days, respectively, is visualized by PAS staining. *a–d* $Mdk^{+/+}$ mice; *e–h* $Mdk^{-/-}$ mice. *a* and *e* pre-injection; *b* and *f* 7 days; *c* and *g* 14 days; *d* and *h* 28 days. Scale bar = 50 μm. **B** The glomerulus (*a*) and the tubulointerstitium (*b*) of $Mdk^{+/+}$ mice at 14 days were visualized by PAS staining. *a* scale bar = 50 μm; *b* scale bar = 100 μm. Semiquantitative analysis of glomerular damage (**C**) and tubulointerstitial injury (**D**). The degrees of both injuries are assessed as described in "Materials and Methods". Data are shown as the mean and SD. *White columns* $Mdk^{+/+}$ mice; *black columns* $Mdk^{-/-}$ mice. *a* $p < 0.05$, *b* $p < 0.01$. $n = 8$ in each group

cells and circulating inflammatory cells in the mesangial areas and capillary lumens, respectively (Fig. 2A, C). The pathological findings in $Mdk^{+/+}$ mice resembled endocapillary proliferative glomerulonephritis. In particular, glomerular capillary lumens in $Mdk^{+/+}$ mice became narrower and obstructed by the various proliferated cells and PAS-positive materials (Fig. 2A-c, B-a). The obstruction was reversible and appeared to be reduced at day 28, during which no treatment was given for an additional 14 days (Fig. 2A-d, h).

Mild tubulointerstitial injury was noted in $Mdk^{+/+}$ mice induced by protein overload at 14 days, as evidenced by

cast formation, and tubular dilation and atrophy accompanied with the detachment of tubular epithelial cells (Fig. 2B-b, D). Both glomerular and tubulointerstitial injuries were consistent with the profile of BUN levels (Figs. 1B, 2C, D).

Electron microscopy

Electron microscopy confirmed these findings with narrowed and obstructed capillary lumens (Fig. 3A), a marked increase of expanded mesangial cells (Fig. 3B), polymorphonuclear leukocytes in the capillary lumens (Fig. 3C, D) and BSA-like depositions in the mesangial areas (Fig. 3B, C) in $Mdk^{+/+}$ mice at 28 days after treatment, although these pathological findings tended to be reversible on PAS staining (Fig. 2A). Podocytes showed a normal appearance (Fig. 3D), whereas focal foot process fusion was occasionally found in both genotypes of mice regardless of BSA treatment (Fig. 3C).

IgG deposition and neutrophils infiltration

Since these pathological findings mentioned above might be also thought of as an infection-related glomerular injury, we assessed the IgG and C3 depositions, hallmarks of inflammation-related glomerulonephritis. We found a trend for enhanced IgG deposition in both the glomeruli and tubulointerstitium of $Mdk^{+/+}$ mice at 14 days (Fig. 4A-a, b), but not at 7 days (data not shown). This deposition was particularly detected on the capillary walls and mesangial areas in glomeruli, and the apical side of tubules. On Western blotting, IgG expression was significantly induced in $Mdk^{+/+}$ mice at 14 days compared with $Mdk^{-/-}$ mice, as seen in the staining (Fig. 4A, C, D). In addition, C3 activation was also more pronounced in glomeruli of $Mdk^{+/+}$ mice compared with that of $Mdk^{-/-}$ mice (Fig. 4B), but not into the tubulointerstitium (data not shown). Furthermore, the number of infiltrating neutrophils into glomeruli was more significant in $Mdk^{+/+}$ mice than $Mdk^{-/-}$ mice at 14 days (Fig. 4E). Interestingly, $Mdk^{+/+}$ mice showed an

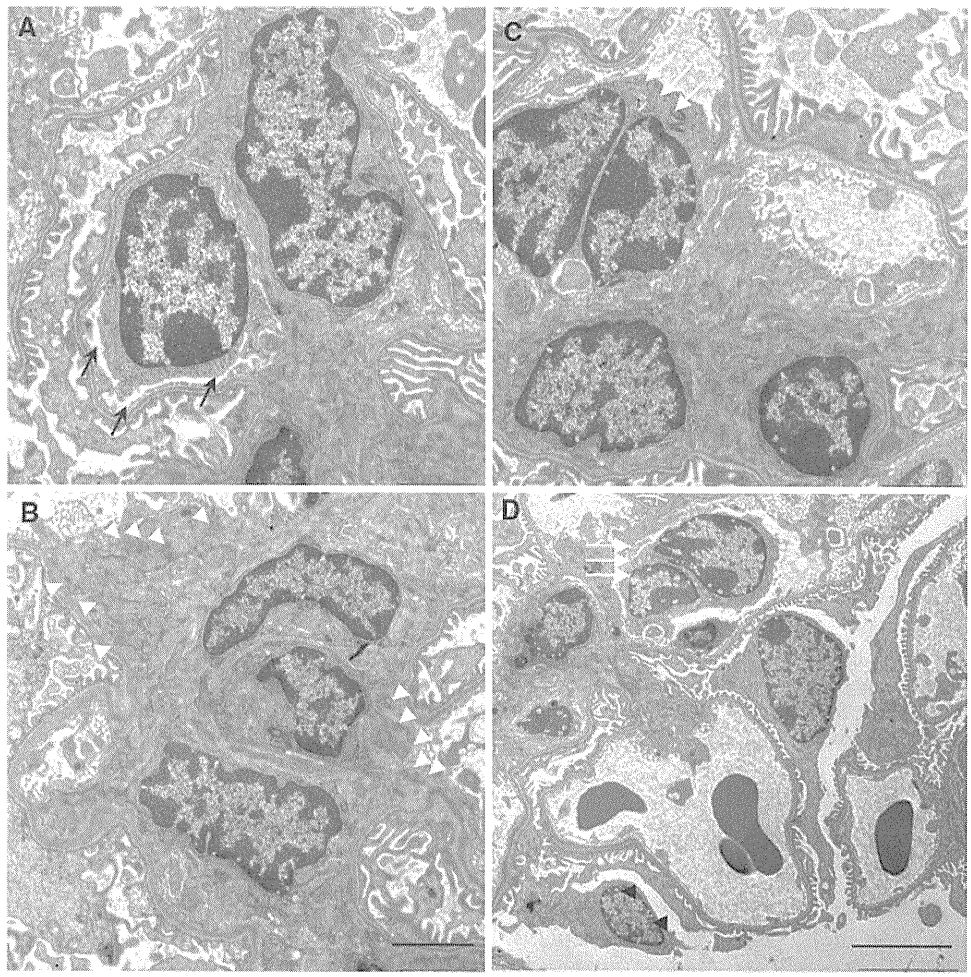

Fig. 3 Glomerular ultrastructure in protein-overload $Mdk^{+/+}$ mice at 28 days after treatment. Representative electron microscopy demonstrated the swelling of glomerular endothelial cells (**A**), the narrowing and obstructed capillary lumens (*black arrow*; **A**, **B**), a marked increase of expanded mesangial cells (**B**), BSA-like depositions in the mesangial areas (*white arrowhead*; **B**, **C**), and polymorphonuclear leukocytes (*white arrow*; **C**, **D**). Podocytes and most foot processes appear normal, although some foot processes are fused (**D**). **A–C** scale bar = 5 μm; **D** scale bar = 10 μm

increase of infiltrating neutrophils at 7 days into the tubulointerstitium, which was, however, noted earlier than into glomeruli (Fig. 4E, F).

MK and chemokine expressions during the development of endocapillary proliferative glomerulonephritis

We examined whether MK expression was associated with other chemokines during the pathogenesis of endocapillary proliferative glomerulonephritis. BSA overload led to a significant increase in MK protein expression at 14 days (Fig. 5A). In particular, MK induction was detected in glomeruli at 14 days after treatment (Fig. 5C). Given previous data [7], it appeared to be located on mesangial cells and endothelial cells. This overall profile was reminiscent of those of both glomerular and tubulointerstitial injuries (Fig. 2). Interestingly, MK induction was found predominantly and concomitantly with IgG and C3 depositions, and neutrophil infiltration in glomeruli.

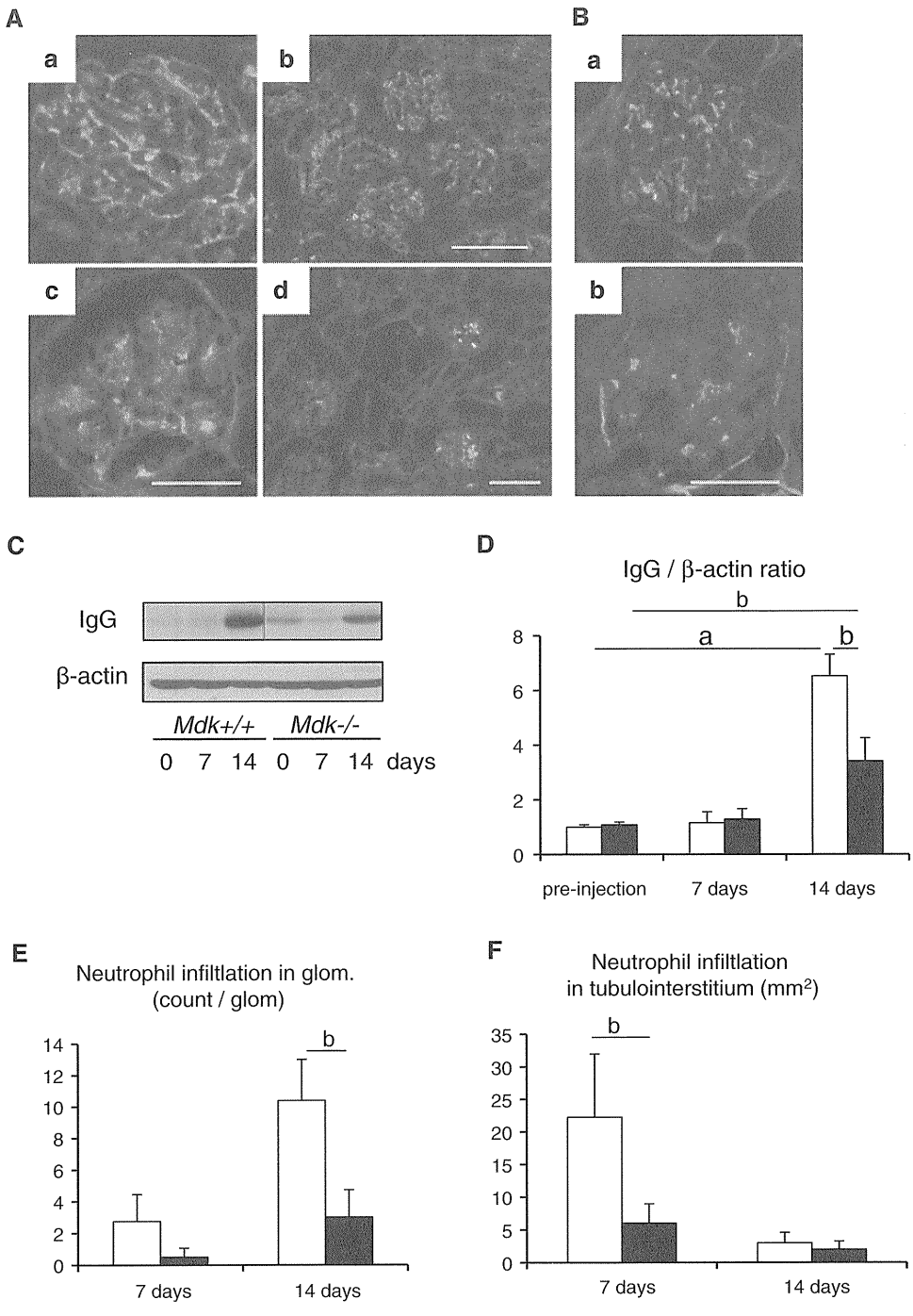

Fig. 4 IgG and C3 depositions, and neutrophil infiltration in protein-overload $Mdk^{+/+}$ and $Mdk^{-/-}$ mice. **A** IgG deposition in the glomerulus (*a*, *c*) and the tubulointerstitium (*b*, *d*) at 14 days are shown by immunofluorescence staining. *a* and *b* $Mdk^{+/+}$ mice; *c* and *d* $Mdk^{-/-}$ mice. *a* and *c* scale bar = 50 μm; *b* and *d* scale bar = 100 μm. **B** C3 deposition in the glomerulus of protein-overload $Mdk^{+/+}$ (*a*) and $Mdk^{-/-}$ (*b*) mice by immunofluorescence staining. Scale bar = 50 μm. **C** Time course of IgG expression, determined by Western blotting. The intensity of IgG bands in (**C**) is normalized to that of β-actin (**D**). The number of neutrophil into the glomerulus (**E**) and tubulointerstitium (**F**) at 0, 7 and 14 days is shown, determined by immunofluorescence staining. Data are shown as the mean and SD. *White columns* $Mdk^{+/+}$ mice; *black columns* $Mdk^{-/-}$ mice. *a* $p < 0.01$, *bp* < 0.05. $n = 8$ in each group